cmgh
CELLULAR AND MOLECULAR GASTROENTEROLOGY AND HEPATOLOGY

ORIGINAL RESEARCH

Desmoplakin Maintains Transcellular Keratin Scaffolding and Protects From Intestinal Injury

Annika Gross,[1] Biaohuan Zhou,[1] Lisa Bewersdorf,[1] Nicole Schwarz,[2] Gabriel M. Schacht,[1] Peter Boor,[3] Konrad Hoeft,[4] Bernd Hoffmann,[5] Elaine Fuchs,[6] Rafael Kramann,[4,7] Rudolf Merkel,[5] Rudolf E. Leube,[2] and Pavel Strnad[1]

[1]Department of Internal Medicine III, University Hospital Aachen, Aachen, Germany; [2]Institute of Molecular and Cellular Anatomy, Rheinisch-Westfälische Technische Hochschule (RWTH) Aachen University, Aachen, Germany; [3]Institute of Pathology, Department of Nephrology, University Hospital Aachen, Aachen, Germany; [4]Department of Medicine II, University Hospital Aachen, Aachen, Germany; [5]Institute of Biological Information Processing 2, Mechanobiology, Forschungszentrum Jülich, Jülich, Germany; [6]Robin Chemers Neustein Laboratory of Mammalian Cell Biology and Development, Howard Hughes Medical Institute, The Rockefeller University, New York, New York; and [7]Institute of Experimental Medicine and Systems Biology, Rheinisch-Westfaelische Technische Hochschule (RWTH) Aachen University, Aachen, Germany

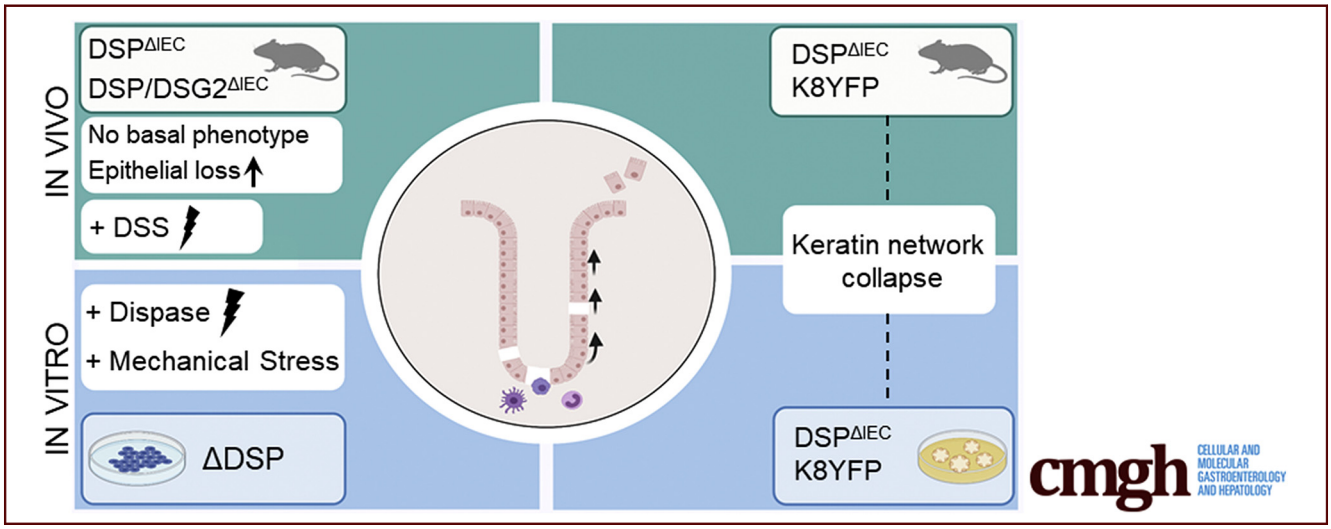

SUMMARY

Analysis of intestine-specific mice lacking desmoplakin or both desmoplakin/desmoglein 2 show that these proteins are dispensable under basal conditions. However, desmoplakin is essential for cell adhesion, mechanical resilience, and proper keratin network organization, and protects from intestinal injury.

BACKGROUND & AIMS: Desmosomes are intercellular junctions connecting keratin intermediate filaments of neighboring cells. The cadherins desmoglein 2 (Dsg2) and desmocollin 2 mediate cell–cell adhesion, whereas desmoplakin (Dsp) provides the attachment of desmosomes to keratins. Although the importance of the desmosome–keratin network is well established in mechanically challenged tissues, we aimed to assess the currently understudied function of desmosomal proteins in intestinal epithelia.

METHODS: We analyzed the intestine-specific villin-Cre DSP ($DSP^{\Delta IEC}$) and the combined intestine-specific DSG2/$DSP^{\Delta IEC}$ (ΔDsg2/Dsp) knockout mice. Cross-breeding with keratin 8–yellow fluorescent protein knock-in mice and generation of organoids was performed to visualize the keratin network. A Dsp-deficient colorectal carcinoma HT29-derived cell line was generated and the role of Dsp in adhesion and mechanical stress was studied in dispase assays, after exposure to uniaxial cell stretching and during scratch assay.

RESULTS: The intestine of $DSP^{\Delta IEC}$ mice was histopathologically inconspicuous. Intestinal epithelial cells, however, showed an accelerated migration along the crypt and an enhanced shedding into the lumen. Increased intestinal permeability and altered levels of desmosomal proteins were detected. An inconspicuous phenotype also was seen in ΔDsg2/Dsp mice. After dextran sodium sulfate treatment, $DSP^{\Delta IEC}$ mice developed more pronounced colitis. A retracted keratin network was seen in the intestinal epithelium of $DSP^{\Delta IEC}$/keratin 8–yellow fluorescent protein mice and organoids derived from these mice presented a collapsed keratin network. The level, phosphorylation status, and solubility of keratins were not affected. Dsp-deficient HT29 cells had an impaired cell adhesion and suffered from increased cellular damage after stretch.

CONCLUSIONS: Our results show that Dsp is required for proper keratin network architecture in intestinal epithelia, mechanical resilience, and adhesion, thereby protecting from injury. *(Cell Mol Gastroenterol Hepatol 2022;13:1181–1200; https://doi.org/10.1016/j.jcmgh.2021.12.009)*

Keywords: Desmosome; Keratin; Apical Junctional Complex; Intestinal Epithelial Barrier; Cell Adhesion.

Keratin intermediate filaments are multifunctional stress-protectors expressed primarily in epithelial cells.[1,2] They are connected through desmosomal cell–cell junctions forming transcellular networks.[3,4] Desmosomes consist of transmembrane components from the desmosomal cadherin families of desmogleins (Dsg) and desmocollins (Dsc) that mediate cell–cell adhesion. In the cytoplasm, they are associated with the armadillo proteins plakophilin and plakoglobin and the plakin member desmoplakin (Dsp), which mediates the attachment to the keratin filament network.[5,6] The desmosome–keratin system is mainly responsible for the stability of epithelial tissues and its function is particularly prominent in mechanically challenged tissues such as the epidermis. In the latter, mutations in keratins lead to a large variety of skin disorders such as epidermolysis bullosa or palmoplantar keratoderma.[2,7] Similarly, auto-antibodies against Dsg/Dsc cause autoimmune blistering diseases such as pemphigus vulgaris, while Dsp mutations were implicated in keratoderma.[8,9] In addition, increasing evidence has shown the importance of the desmosome–keratin system in mechanically less challenged glandular and single-layered epithelia. For example, mutations in keratin (K)8/K18, the major keratin family members expressed in simple epithelia, increased the susceptibility to advanced liver disease.[10] An intronic variant in the *Dsp* gene that results in diminished Dsp levels is the most established genetic risk factor predisposing to idiopathic pulmonary fibrosis.[11] Although the biological role of K8/K18 variants in inflammatory bowel disease remains to be clarified,[12] altered desmosomal protein levels are seen in individuals with inflammatory bowel disease and these changes may contribute to the impaired intestinal barrier seen in Crohn's disease.[13–15] These data are supported by findings in multiple transgenic models. Among them, K8 knockout mice show spontaneous colitis,[16] while loss of Dsg2, the only Dsg produced in intestinal epithelial cells, is well tolerated under basal conditions, but leads to increased susceptibility to both chemical and microbial injury.[13] To further elucidate the biological role of the keratin-desmosome system in the intestine, we turned to Dsp knockout animals. Although Dsp is essential for epidermal sheet formation,[17] intestine-specific Dsp knockout ($DSP^{\Delta IEC}$) mice did not show an obvious phenotype under basal conditions. This was somewhat surprising given that intestinal epithelial-specific loss of plectin, another cytolinker connecting keratin filaments with cell junctions, led to spontaneous colitis.[18] Therefore, we decided to systematically study the impact of Dsp loss on keratin network architecture as well as the susceptibility to intestinal injury. To that end, $DSP^{\Delta IEC}$ mice were cross-bred with the reporter K8-yellow fluorescent protein (YFP) knock-in mouse[19] or subjected to dextran sodium sulfate (DSS)-induced colitis. Mating of $DSP^{\Delta IEC}$ mice with an intestinal-specific Dsg2 knockout ($DSG2^{\Delta IEC}$) was used to evaluate the consequence of a combined desmosomal defect. In summary, we show that Dsp is required for keratin network organization, epithelial adhesion, and the protection of intestinal epithelial cells from mechanical and chemical injury.

Results

To study the biological relevance of Dsp in the intestine, we generated intestinal epithelium–specific Dsp knockout mice ($DSP^{\Delta IEC}$). In line with previous findings,[20] $DSP^{\Delta IEC}$ mice showed an efficient deletion of Dsp in both jejunum and colon, while no Dsp loss was observed in other organs such as stomach, liver, and heart (Figures 1*A* and *B* and 2). Immunofluorescence staining of colonic tissue confirmed the loss of Dsp and showed a normal distribution of other desmosomal proteins (Figure 1*C*). Biochemical analysis showed decreased levels of Dsg2 and plakoglobin (PG), while the amounts of other desmosomal proteins were unaltered (Figure 1*D* and *E*). These changes seemed to occur post-transcriptionally given that there were no differences in the Dsg2/PG messenger RNA (mRNA) levels (Figure 3). $DSP^{\Delta IEC}$ mice developed normally; displayed normal body weight, colonic and small intestinal length; and had no diarrhea (Figure 4*A*). No inflammation was seen and this finding was supported by unaltered expression of the proinflammatory cytokines tumor necrosis factor α, interleukin (IL)1β, and IL6 (Figure 4*B* and *C*). Histologic evaluation showed a morphologically inconspicuous small and large intestine (Figure 5*A* shows large intestine; pictures from small intestine are not shown). Electron microscopy showed normal-appearing desmosomal plaques in the colon (Figure 5*B*). Notably, $DSP^{\Delta IEC}$ animals showed somewhat increased intestinal permeability for 4 kilodaltons fluorescein isothiocyanate (FITC) dextran (Figure 5*C*). Accelerated migration of 5-bromo-2-deoxyuridine (BrdU)-labeled colonic cells along the crypt axis was seen 24 hours after BrdU injection (Figure 6*A*). In line with the increased cellular turnover, Dsp-deficient animals harbored a higher epithelial cell content in the intestinal lumen as indicated by the increased amount of the epithelial cell marker K8

Abbreviations used in this paper: **Agr2, anterior gradient 2; BrdU, 5-bromo-2-deoxyuridine; BSA, bovine serum albumin; Dsc, desmocollin; Dsg, desmoglein; Dsp, desmoplakin; DSS, dextran sodium sulfate; FITC, fluorescein isothiocyanate; fl, floxed; GFP, green fluorescent protein; IEC, intestinal epithelial cells; IL, interleukin; K, keratin; mRNA, messenger RNA; PAS, periodic acid–Schiff; PBS, phosphate-buffered saline; PG, plakoglobin (γ-catenin); SDS, sodium dodecyl sulfate; WT, wild-type; YFP, yellow fluorescent protein.**

Most current article

2352-345X
https://doi.org/10.1016/j.jcmgh.2021.12.009

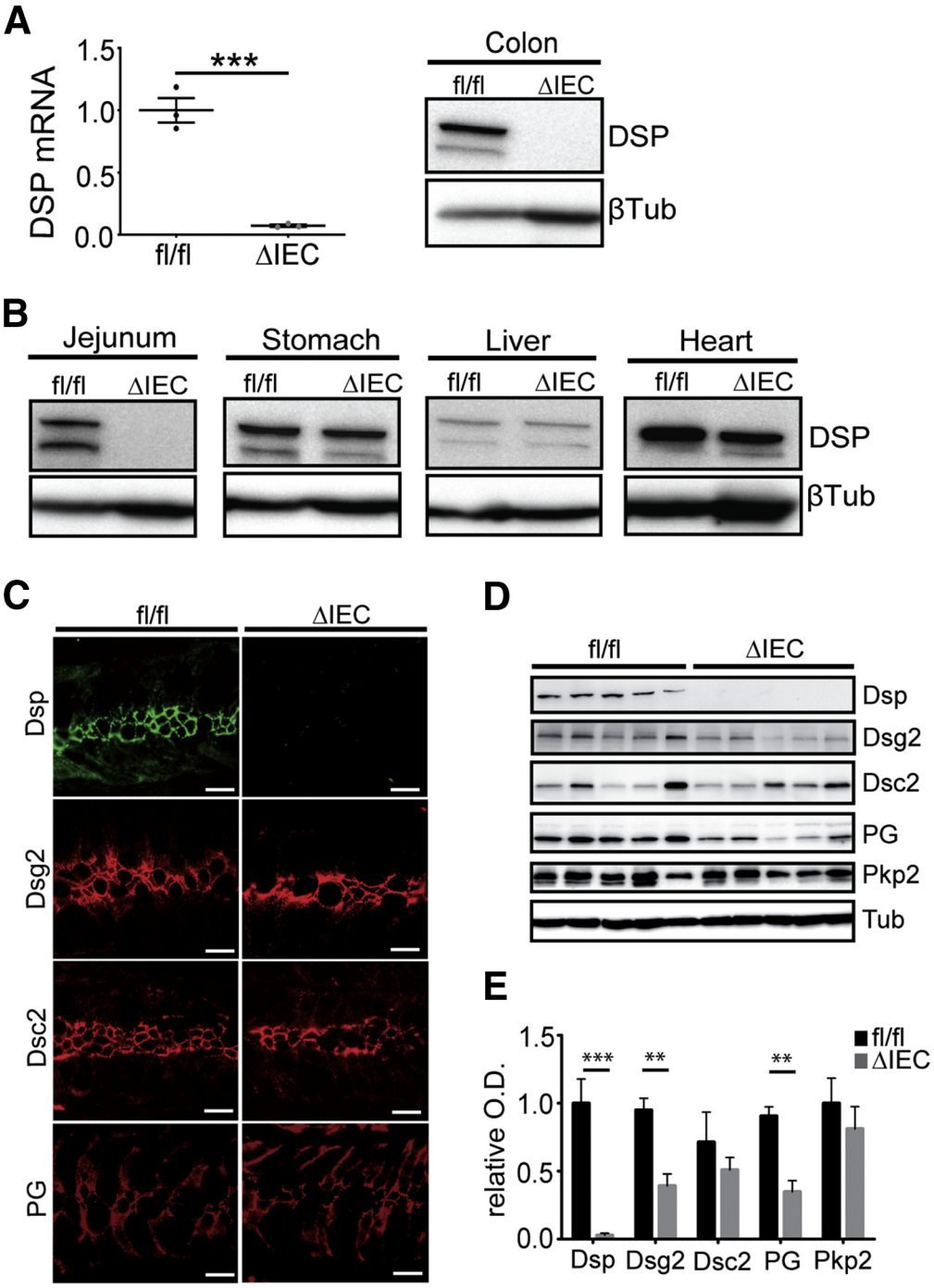

Figure 1. DSP-deficient animals (*DSP*$^{\Delta IEC}$) showed an intestine-specific Dsp loss and an altered desmosomal protein composition. (*A* and *B*) *DSP* mRNA and protein levels were evaluated by real-time reverse-transcription polymerase chain reaction (n = 3) and immunoblotting in the delineated organs of 10-week-old, sex-matched *DSP*$^{\Delta IEC}$ (ΔIEC) and DSP$^{fl/fl}$ (fl/fl) mice. The *L7* (mouse ribosomal protein) gene and β-tubulin (βTub) were used as an internal and loading control, respectively. (*C*) The distribution of Dsp, Dsg2, Dsc2, and PG in the colons of 10-week-old, sex-matched DSP$^{\Delta IEC}$ (ΔIEC) mice and their floxed littermates (fl/fl) was visualized by immunofluorescence. *Scale bars*: 20 μm. (*D* and *E*) The impact of Dsp loss on colonic desmosomal composition was analyzed by immunoblotting (n = 5). β-tubulin was used as a loading control. The optical density (OD) values from immunoblots were normalized to the OD values of β-tubulin. A 2-tailed Student *t* test was used for statistical analyses. $^{**}P < .01$, $^{***}P < .001$. Similar results were obtained in male and female mice. Pkp2, plakophilin 2.

(Figure 6*B*). The analysis of selected differentiation/lineage markers showed an inapparent stem cell differentiation pattern (Figure 7). To explore the impact of aging, we systematically analyzed 52-week-old animals. DSP$^{\Delta IEC}$ mice had normal body weights, colon lengths, and small intestinal lengths (Figure 8*A*). Histologic staining showed a regular colonic structure, while periodic acid–Schiff (PAS) staining and immunohistochemical staining for anterior gradient 2 (Agr2) showed an unaltered number of goblet cells (Figure 8*B*). No colonic inflammation was noted within the groups as confirmed by unchanged levels of cytokines tumor necrosis factor α and IL1β (Figure 8*C*). Because neither a loss of a desmosomal cadherin[13] nor a Dsp deficiency in intestinal epithelial cells led to an obvious phenotype under basal conditions, we wondered about an impact of a combined defect. To that end, we generated mice with a deletion of both Dsg2 and Dsp in the intestinal epithelia (ΔDsg2/Dsp). Biochemical analysis confirmed the efficient deletion of both desmosomal proteins (Figure 9). ΔDsg2/Dsp animals (age, 28 wk) developed normally and no changes in

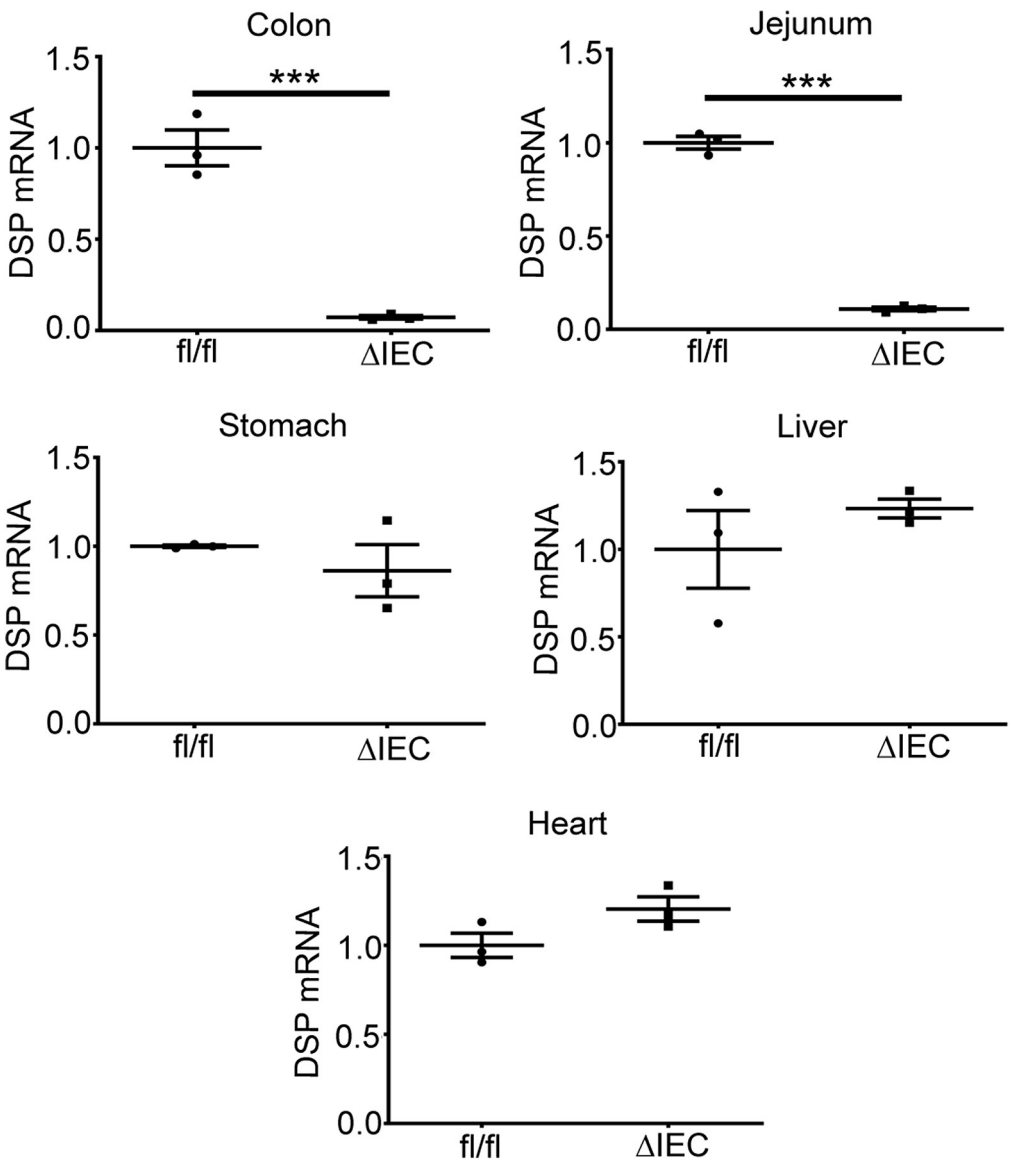

Figure 2. DSP-deficient animals (*DSP*$^{\Delta IEC}$) showed an efficient intestine-specific Dsp loss. *DSP* mRNA levels were quantified in the highlighted mouse organs of 10-week-old, sex-matched *DSP*$^{\Delta IEC}$ (ΔIEC) and DSP$^{fl/fl}$ (fl/fl) mice by real-time reverse-transcription polymerase chain reaction and shown as dot plots (n = 3). The *L7* (mouse ribosomal protein) gene was used as an internal control. Average mRNA expression in fl/fl mice was set arbitrarily as 1 and levels in ΔIEC mice are presented as a ratio. A 2-tailed Student *t* test was used for statistical analyses. ***$P < .001$. Similar results were obtained in male and female mice.

body weight or in the colon and small intestinal lengths were detected (Figure 10*A*). Histology illustrated an unaltered colon architecture and a comparable amount of goblet cells in all analyzed genotypes. The latter observation was confirmed by similar mRNA expression of the goblet cell marker mucin 2 (Figure 10*B*). Furthermore, no inflammation was noted as shown by similar levels of proinflammatory cytokines (Figure 10*C*). Gavage with 4 kilodaltons FITC-labeled dextran showed only a moderate increase in intestinal permeability (Figure 10*D*). To test the importance of Dsp during intestinal stress, we challenged DSP$^{\Delta IEC}$ mice and their floxed littermates with DSS. Compared with DSP$^{fl/fl}$ mice, DSP$^{\Delta IEC}$ animals experienced increased weight loss with profound fecal bleeding and a significantly reduced colon length (Figure 11*A*–*C*). Histologic examination showed massive tissue destruction in DSS-treated Dsp-deficient mice with marked epithelial cell loss, edema, and inflammatory cell infiltration that translated into increased injury scores (Figure 11*D*). The profoundly intensified inflammation was corroborated by increased levels of the analyzed proinflammatory cytokines (Figure 11*E*).

Given that Dsp mediates the connection between desmosomes and keratin intermediate filaments, we assessed the consequences of Dsp loss on keratin organization. Under basal conditions, DSP$^{\Delta IEC}$ and DSP$^{fl/fl}$ mice showed similar mRNA and protein levels of K7, K8, K18, and K19 (Figure 12*A* and *B*). No differences in K8 solubility were noted (Figure 12*C*). In line with that, phosphorylation of K8 at S79 and S432 did not differ significantly among the phenotypes (Figure 12*C* and data not shown). To better delineate keratin network organization in vivo, DSP$^{\Delta IEC}$ and DSP$^{fl/fl}$ mice were cross-bred with knock-in animals expressing the YFP-tagged version of K8.[19] Confocal laser scanning microscopy showed a normal-appearing K8 network in the colon and jejunum of DSP$^{fl/fl}$ mice, with K8

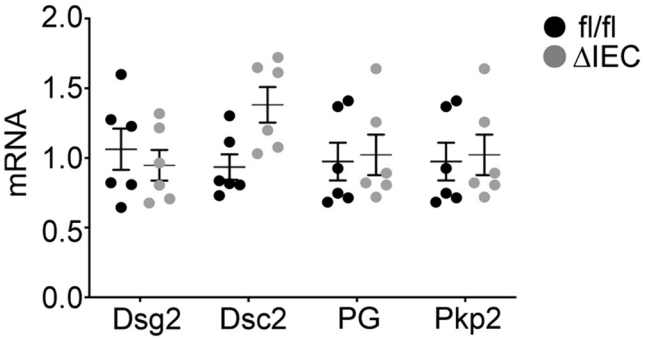

Figure 3. DSP-deficient animals (DSP$^{\Delta IEC}$) showed no alterations in the expression of desmosomal components. The impact of Dsp loss on colonic desmosomal composition was analyzed in 10-week-old, sex-matched DSP$^{\Delta IEC}$ (ΔIEC) mice and their floxed littermates (fl/fl) by real-time reverse-transcription polymerase chain reaction (n = 6) and shown as dot plots. The *L7* (mouse ribosomal protein) gene was used as an internal control. Average mRNA expression in fl/fl mice was set arbitrarily as 1 and levels in ΔIEC mice are presented as a ratio. Similar results were obtained in male and female mice. Pkp2, plakophilin 2.

being located in close contact with the plasma membrane. Loss of Dsp resulted in a retracted network that became apparent as a wider distance between the keratin rings, and was even more pronounced in the jejunum (Figure 13*A–C*). To further explore keratin distribution in rapidly growing intestinal epithelia, we turned to small intestinal organoids. Although the loss of Dsp did not visibly alter the growth and development of the organoids, a dramatic disruption of the keratin network occurred in DSP$^{\Delta IEC}$ organoids. They showed a profoundly disorganized, collapsed network (Figure 13*D*), which was in strong contrast to the cortical pattern seen in DSP$^{fl/fl}$ organoids.

Given the known importance of keratins for mechanical stability, we compared the mechanical resilience of wild-type colorectal carcinoma–derived HT29 cells and HT29 cells with a deleted Dsp exon 8 (ΔDSP). The complete loss of Dsp was confirmed on both the mRNA and protein level (Figure 14*A* and *B*), and the efficient expression of the targeting vector was corroborated by the incorporated green fluorescent protein (GFP) fluorescence (Figure 14*C*). No changes in cell growth or morphology compared with wild-type (WT) HT29 cells were observed (Figure 14*C* and not shown). An inconspicuous cellular monolayer was seen in ΔDSP cells by H&E and phalloidin stainings (Figure 15*A* and data not shown). Immunofluorescence staining showed an unperturbed localization of the desmosomal cadherin Dsg2 (Figure 14*D*). Nevertheless, mechanical stress resulted in a more profound fragmentation of the epithelial sheets in Dsp-deficient cells compared with their WT counterparts

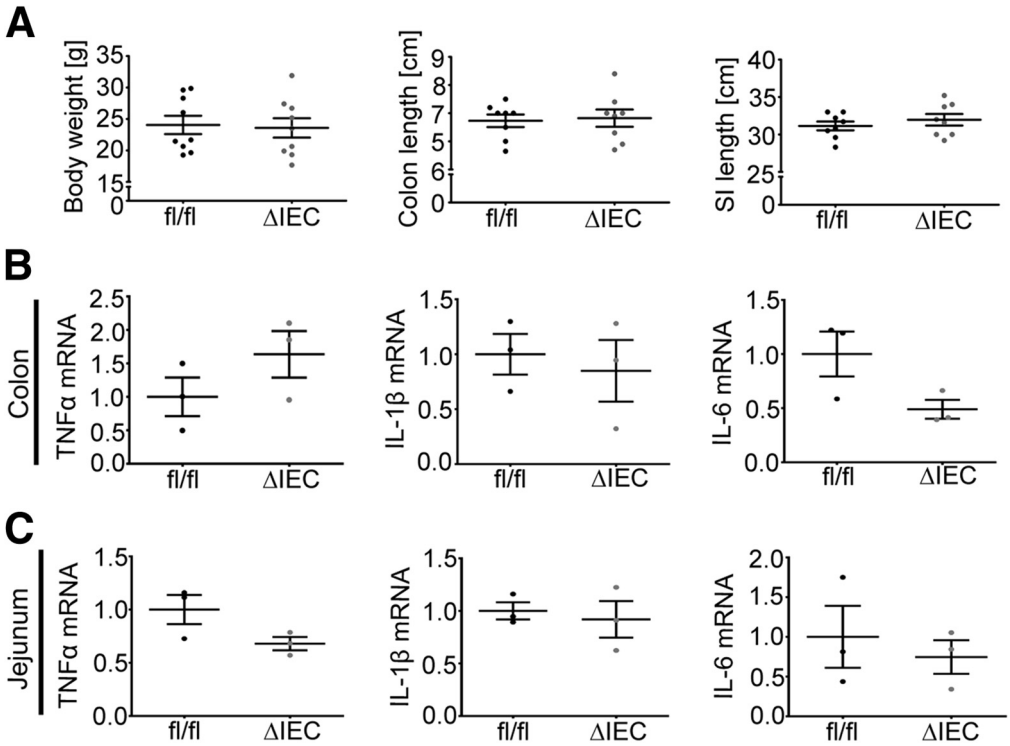

Figure 4. DSP-deficient animals (DSP$^{\Delta IEC}$) developed normally and showed no obvious intestinal inflammation under basal conditions. (*A*) The body weights, as well as colon and small intestinal (SI) lengths of 10-week-old, sex-matched DSP$^{\Delta IEC}$ (ΔIEC) mice and their floxed littermates (fl/fl) are shown as dot plots (n = 7–9). (*B,C*) The inflammatory cytokines tumor necrosis factor α (*TNFα*), *IL-1β*, and *IL-6* were assessed in the colon and jejunum of both groups by real-time reverse-transcription polymerase chain reaction (n = 3). The *L7* (mouse ribosomal protein) gene was used as an internal control. Average mRNA expression in fl/fl mice was set arbitrarily as 1 and levels in ΔIEC mice are presented as a ratio. Similar results were obtained in male and female mice.

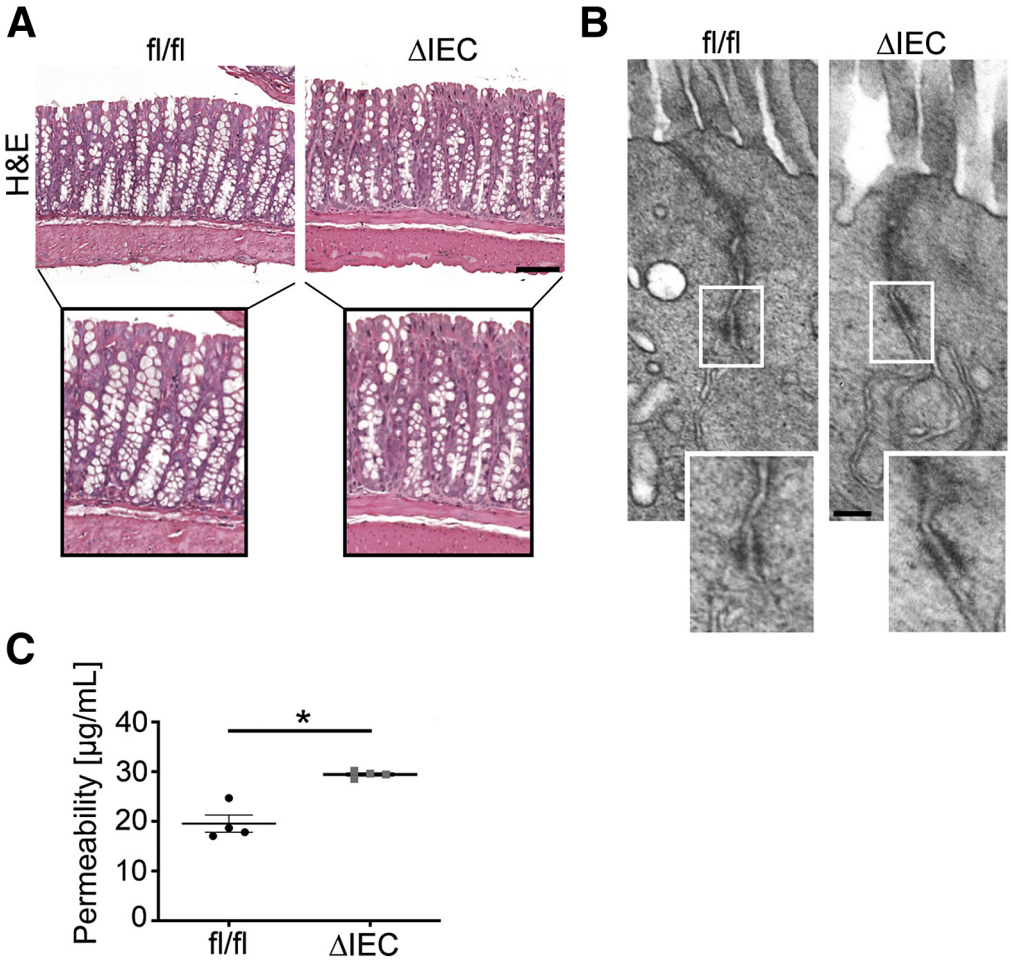

Figure 5. Loss of Dsp leads to increased intestinal permeability. (*A*) H&E staining highlights the overall colon morphology in 10-week-old, sex-matched DSP$^{\Delta IEC}$ (ΔIEC) mice and their floxed littermates (fl/fl). *Scale bar*: 100 μm. (*B*) Desmosomal ultrastructure was assessed in both groups by electron microscopy. *Scale bar*: 100 nm. (*C*) Serum levels of 4-kilodalton FITC-dextran were quantified in 10-week-old, sex-matched mice 4 hours after the gavage (n = 4). The data are represented as dot plots. A 2-tailed Student *t* test was used for statistical analyses. *$P < .05$. Similar results were obtained in male and female mice.

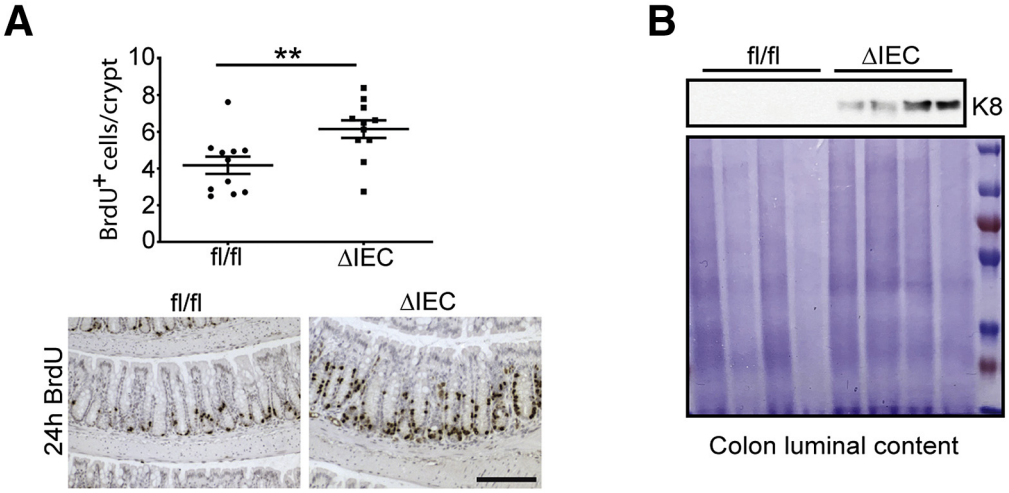

Figure 6. DSP-deficient animals (DSP$^{\Delta IEC}$) showed an accelerated epithelial migration and a higher epithelial loss. (*A*) Ten-week-old, sex-matched DSP$^{\Delta IEC}$ (ΔIEC) mice and their floxed littermates (fl/fl) were injected with BrdU and the amount of BrdU-positive cells was quantified 24 hours later (n = 11). *Scale bar*: 200 μm. (*B*) Immunoblotting for the epithelial cell marker K8 in the colonic luminal content of 10-week-old, sex-matched mice was performed as a marker of epithelial extrusion (n = 4). Coomassie staining was used as a loading control. A 2-tailed Student *t* test was used for statistical analyses. **$P < .01$. Similar results were obtained in male and female mice.

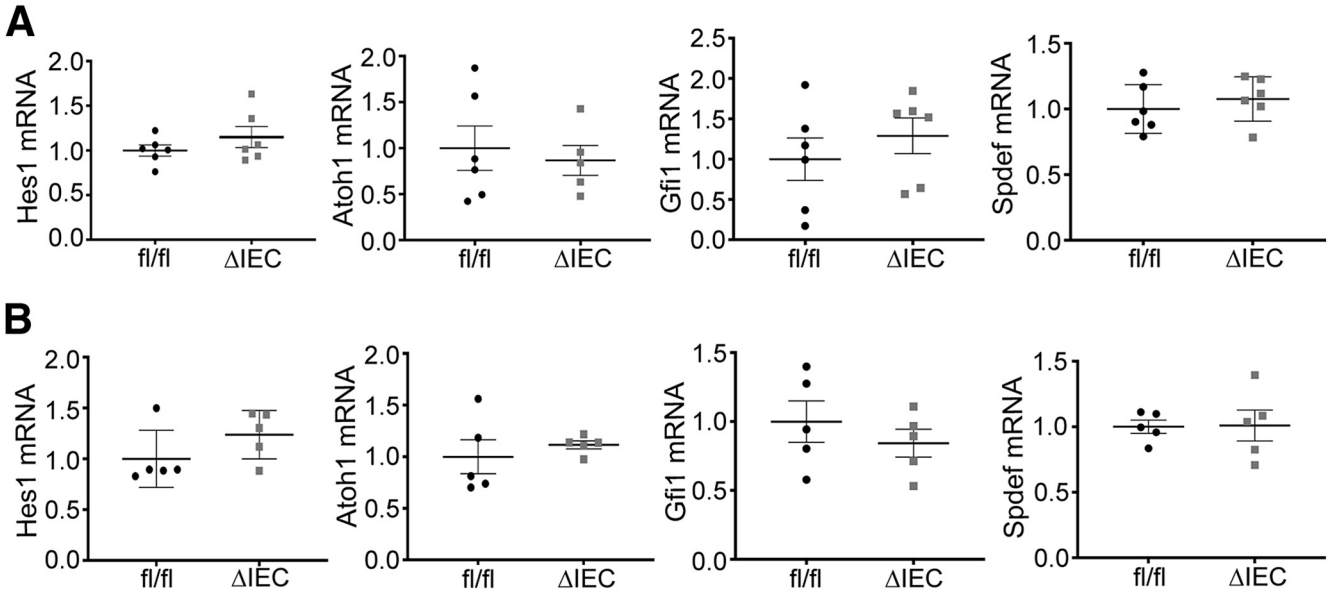

Figure 7. DSP-deficient animals (DSP$^{\Delta IEC}$) showed no abnormalities in cellular differentiation. mRNA levels of secretory lineage markers *Atoh1*/*Hes1* and cell maturation markers *Gfi1*/*Spdef* were quantified in the (*A*) colon and (*B*) jejunum of 10-week-old, sex-matched DSP$^{\Delta IEC}$ (ΔIEC) and DSP$^{fl/fl}$ (fl/fl) mice by real-time reverse-transcription polymerase chain reaction (n = 5–6). The *L7* (mouse ribosomal protein) gene was used as an internal control. Average mRNA expression in fl/fl mice was set arbitrarily as 1 and levels in ΔIEC mice are presented as a ratio. All data are represented as dot plots. Similar results were obtained in male and female mice.

(Figure 14*E*). Similarly, uniaxial cyclic cell stretching led to a more obvious monolayer disruption in ΔDSP vs WT cells (Figure 14*F*). Moreover, Dsp-deficient cells showed a stronger release of the cellular damage marker lactate dehydrogenase into the cell supernatant (Figure 14*F*). In contrast, loss of Dsp did not affect the wound healing response determined by a scratch assay (Figure 15*B*). In summary, our results show that Dsp is largely dispensable in unstressed intestinal epithelia, but it is crucial for keratin network organization, cellular adhesion, and tissue integrity, and thereby for coping with intestinal stress (Figure 16).

Discussion

Our study analyzed the role of the desmosome–keratin system in the intestine. We showed that loss of Dsp did not influence the formation of normal-appearing desmosomes, which is in line with previous data.[20] The fact that Dsp is necessary for desmosomal integrity in the epidermis but less so in the intestine[17,20] suggests that it is more important in mechanically challenged tissues. This is not surprising because Dsp becomes mechanically loaded only when cells are exposed to external mechanical stresses.[21] Although no intestinal injury was noted, DSP$^{\Delta IEC}$ mice showed decreased Dsg2 and PG protein levels. These data are in line with observations in Dsg2-deficient animals[13] and indicate that alterations in desmosomal proteins affect the post-translational regulation of other desmosomal components. Similarly, cardiac-specific ablation of Dsp resulted in decreased levels of cytosolic PG.[22] Further studies are needed to delineate the underlying molecular mechanisms.

The alterations observed in unchallenged DSP$^{\Delta IEC}$ mice included an increased intestinal permeability, a faster migration along the crypt–villus axis, and a stronger epithelial turnover, which indicates the importance for epithelial adhesion. Similar findings were made after the loss of desmosomal components Dsc2 and Dsg2, which lead to impaired intestinal adhesion.[14,15] The increased epithelial shedding into the intestinal lumen that was observed in DSP$^{\Delta IEC}$ mice is compatible with the animals with intestine-specific plectin deletion that show increased cellular turnover and a trend toward higher epithelial detachment.[18]

The fact that Dsp is crucial for cellular adhesion was supported further by our in vitro studies highlighting a higher cell mechanical fragility of Dsp-deficient cells. In addition to Dsp, keratins constitute important mechanical stabilizers and keratin mutations result in cellular fragility.[23] Despite that, neither an isolated Dsp loss nor a combined deletion of Dsp and Dsg2 resulted in a spontaneous intestinal injury. This finding extends earlier observations[13,24,25] and suggests that loss of desmosomal proteins can be functionally compensated in unchallenged intestinal epithelia. These rather minor functional defects were somewhat surprising because the cross-breeding of DSP$^{\Delta IEC}$ animals with K8–YFP mice showed that Dsp loss results in a profoundly disorganized keratin filament network in the small and large intestine. Even stronger alterations were seen in the rapidly growing intestinal organoids. Further studies are needed to dissect the importance of Dsp in these situations as well as to delineate its role in the small vs large intestine.

Collectively, these data indicate that Dsp is essential for the tethering of keratins in these cells and cannot be

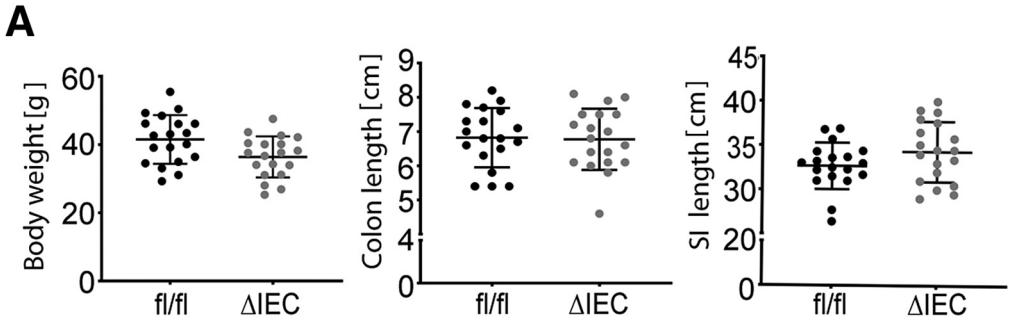

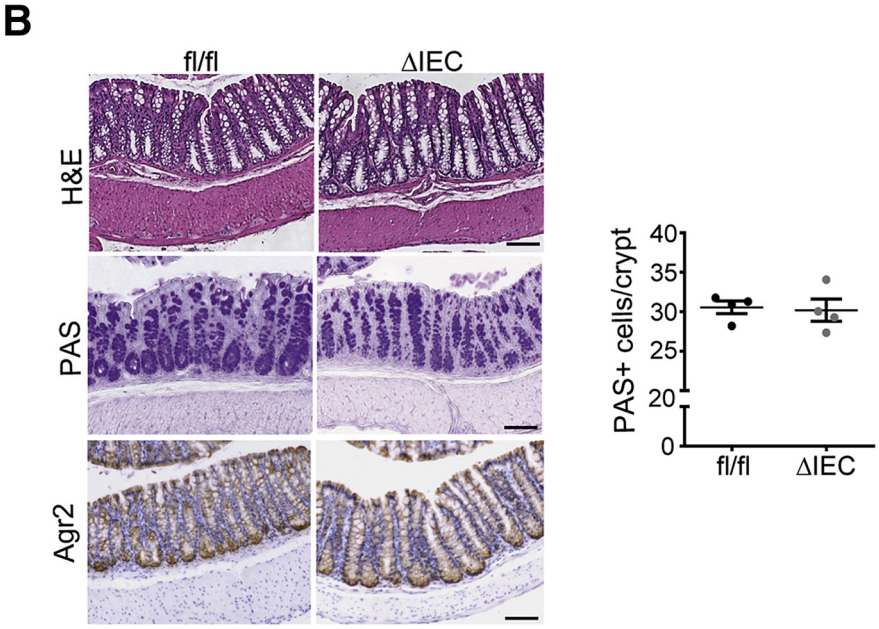

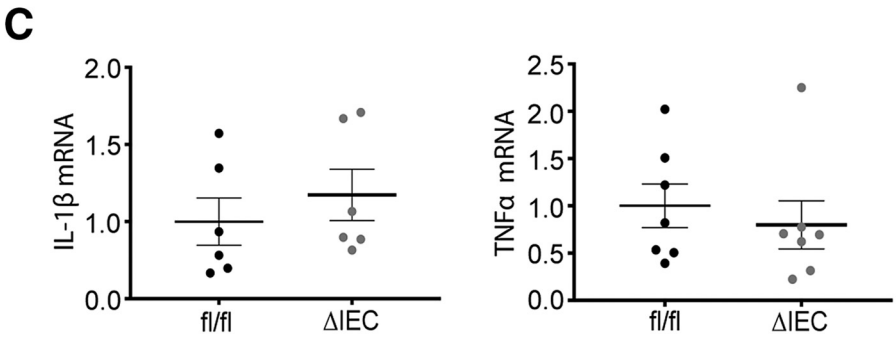

Figure 8. DSP-deficient animals ($DSP^{\Delta IEC}$) (age, 52 wk) showed no obvious phenotype under basal conditions. (*A*) The body weights, colon lengths, and small intestinal (SI) lengths were analyzed in 52-week-old, sex-matched $DSP^{\Delta IEC}$ (ΔIEC) and $DSP^{fl/fl}$ (fl/fl) mice. The data are shown as dot plots (n = 19). (*B*) H&E staining showed the overall colonic architecture. PAS staining and Agr2 immunohistochemical staining visualize the goblet cells. *Scale bar*: 100 μm (*C*) Real-time reverse-transcription polymerase chain reaction quantifies the colonic levels of the cytokines tumor necrosis factor α (*TNF*α) and *IL-1*β (n = 6–7) as a surrogate of inflammation. The *L7* (mouse ribosomal protein) gene was used as an internal control. Average mRNA expression in fl/fl mice was set arbitrarily as 1 and levels in ΔIEC mice represent a ratio. Similar results were obtained in male and female mice.

compensated by other cytolinkers. In line with that, Dsp absence or mutation in keratinocytes led to a retracted keratin network after mechanical stress.[25–27] Furthermore, it has been shown that modifications in the keratin–desmosome interaction alter cell stiffness in human epithelial cells.[28] However, despite the lost transcellular connection, the retained keratins still seem to fulfill important cellular functions because the phenotype of $DSP^{\Delta IEC}$ mice is markedly less severe than the phenotype seen in K8 knockout mice.[12] Notably, keratins are multifunctional proteins fulfilling various nonmechanical functions,[2,29,30] and these retained functions likely are responsible for the comparably mild phenotype of $DSP^{\Delta IEC}$ animals. Finally, our data show that desmoplakin is more dispensable than its related cytolinker plectin because intestinal deletion of plectin led to spontaneous colitis.[18] This is not surprising because plectin fulfills a much broader spectrum of functions than desmoplakin and its deletion results in dysfunctional hemidesmosomes and intercellular junctions[18] that are not affected by desmoplakin loss. On the

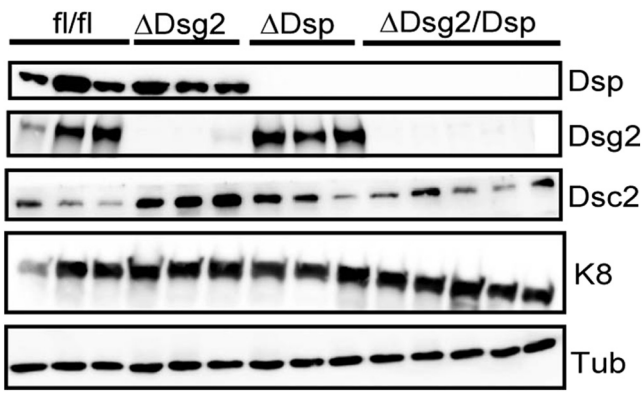

Figure 9. DSG2/DSP-deficient animals (ΔDsg2/Dsp) showed an intestine-specific Dsg2 and Dsp loss. The colonic levels of the depicted proteins were assessed in $DSG2^{\Delta IEC}$ (ΔDsg2) or $DSP^{\Delta IEC}$ (ΔDsp) single-knockout, $DSG2/DSP^{\Delta IEC}$ (ΔDsg2/Dsp) double-knockout mice and their floxed littermates (fl/fl) by immunoblotting (n = 3–5). β-tubulin (Tub) was used as a loading control. Similar results were obtained in male and female mice.

other hand, deletion of epiplakin, a cytolinker with more restricted cellular junctions, did not lead to an obvious intestinal phenotype either.[31] Although the moderate intestinal permeability seen in untreated $DSP^{\Delta IEC}$ animals is not sufficient to induce epithelial injury, it may promote the disruption of the intestinal barrier during DSS colitis. As an underlying mechanism, proinflammatory cytokines are known to weaken the epithelial junctions[32] and thereby may perpetuate the vicious cycle of disturbed epithelial barrier and injury.[33] A similar mechanism was postulated in $DSG2^{\Delta IEC}$ mice[13] and multiple cellular models.[34,35]

In summary, our findings support an important role of Dsp for epithelial tissue integrity. Because its loss results in impaired attachment of keratins to desmosomes as well as alterations in desmosomal protein levels, Dsp seems to be important for both. Although desmosomal proteins are dispensable under basal conditions, they may constitute an important second line of defense during intestinal stress. Previous data from patients with idiopathic pulmonary fibrosis suggest that decreased expression of Dsp caused by intronic variant rs2076295 may predispose to development of injury in single-layered epithelia.[11] Together with our data, these findings should spur a systematic analysis of this variant in individuals with digestive disorders.

Materials and Methods

Mouse Experiments

Mice with intestine-specific deletion of Dsp and Dsg2, as well as combined deletion of both genes (ΔDsg2/Dsp), were generated by crossing previously described DSG2 exons 4/5 floxed ($DSG2^{fl/fl}$) and DSP exon 2 floxed ($DSP^{fl/fl}$) mice with animals expressing Cre under the control of the villin promotor ($DSG2^{\Delta IEC}/DSP^{\Delta IEC}$).[13,20] $DSP^{\Delta IEC}$ animals were further cross-bred with previously described K8–YFP knock-in mice.[19] All mice were on a C57BL/6 background, were co-housed, and kept under standardized conditions (12 hours day/night cycle; 21°C–24°C; humidity, ~50%) with free access to food and water. To induce colitis, 10-week-old sex-matched mice were exposed to 2% DSS (MP Biochemicals, Heidelberg, Germany) in drinking water for 5 days followed by a switch to normal water. The animals were killed with an isoflurane overdose on day 7. Untreated, co-housed, age- and sex-matched littermates were used as controls. Rectal bleeding was evaluated using a commercial hemoCARE fecal occult blood guaiac test (Care diagnistica, Voerde, Germany). Semiquantitative scoring from 0 to 3 (0, no bleeding; 1, mild bleeding; 2, moderate bleeding; and 3, severe bleeding) was performed. All intestinal parts were washed with 1× phosphate-buffered saline (PBS). Proximal parts were stored as Swiss rolls in 4% formaldehyde overnight for histologic evaluation or frozen in OCT compound (Tissue-Tek; Sakura, Staufen, Germany) for cryosectioning. Distal parts and samples from other organs were snap-frozen in liquid nitrogen for protein and RNA analysis. To examine intestinal permeability, mice were fasted for 3 hours and subsequently gavaged with 0.6 mg/g of body weight 4-kilodalton FITC-labeled dextran (Sigma-Aldrich, Steinheim, Germany). Four hours later, blood was collected retroorbitally and the fluorescence intensity in serum was quantified (excitation, 492 nm; emission, 525 nm; Cytation3 imaging reader; BioTek, Bad Friedrichshall, Germany). The samples were prepared in duplicates and the results were calculated according to the standard curve. To label proliferating cells, 50 μg/g of body weight BrdU (Sigma-Aldrich) was injected intraperitoneally.

Generation of Organoids From Isolated Small Intestinal Stem Cells

Small intestines were removed, washed with ice-cold PBS, and cut into 3-cm–long pieces that were opened longitudinally. The villi were scraped off with a coverslip and the remaining tissue fragments were washed with PBS. Afterward, they were incubated in 1 mmol/L EDTA/PBS solution for 30 minutes at 4°C on a tube roller and transferred to 5 mmol/L EDTA/PBS for 1 hour at 4°C to enrich for small intestinal crypts. The crypt-containing solution was filtered through a 70-μm cell strainer, the crypts were counted, and centrifuged at 300 × g for 5 minutes at 4°C. The crypt-containing pellet was resuspended in a Matrigel matrix (Corning, Kaiserslautern, Germany) and seeded into a prewarmed 48-well plate. Matrigel was allowed to polymerize for 15 minutes at 37°C and the crypts were overlayed with Advanced Dulbecco's modified Eagle medium/F12 supplemented with 1% Glutamax, 1% 1 mol/L HEPES, and 1% penicillin/ streptomycin, containing 1× N2, 1× B27 supplement (both from Invitrogen, Waltham, MA), 1.25 mmol/L n-acetylcysteine (Sigma-Aldrich), 0.05 μg/mL mouse epidermal growth factor (Invitrogen), 0.1 μg/mL murine Noggin (Peprotech, Hamburg, Germany), and 1 μg/mL recombinant human R-Spondin 1 (R&D Systems, Minneapolis, MN). The medium was changed every 3 days and

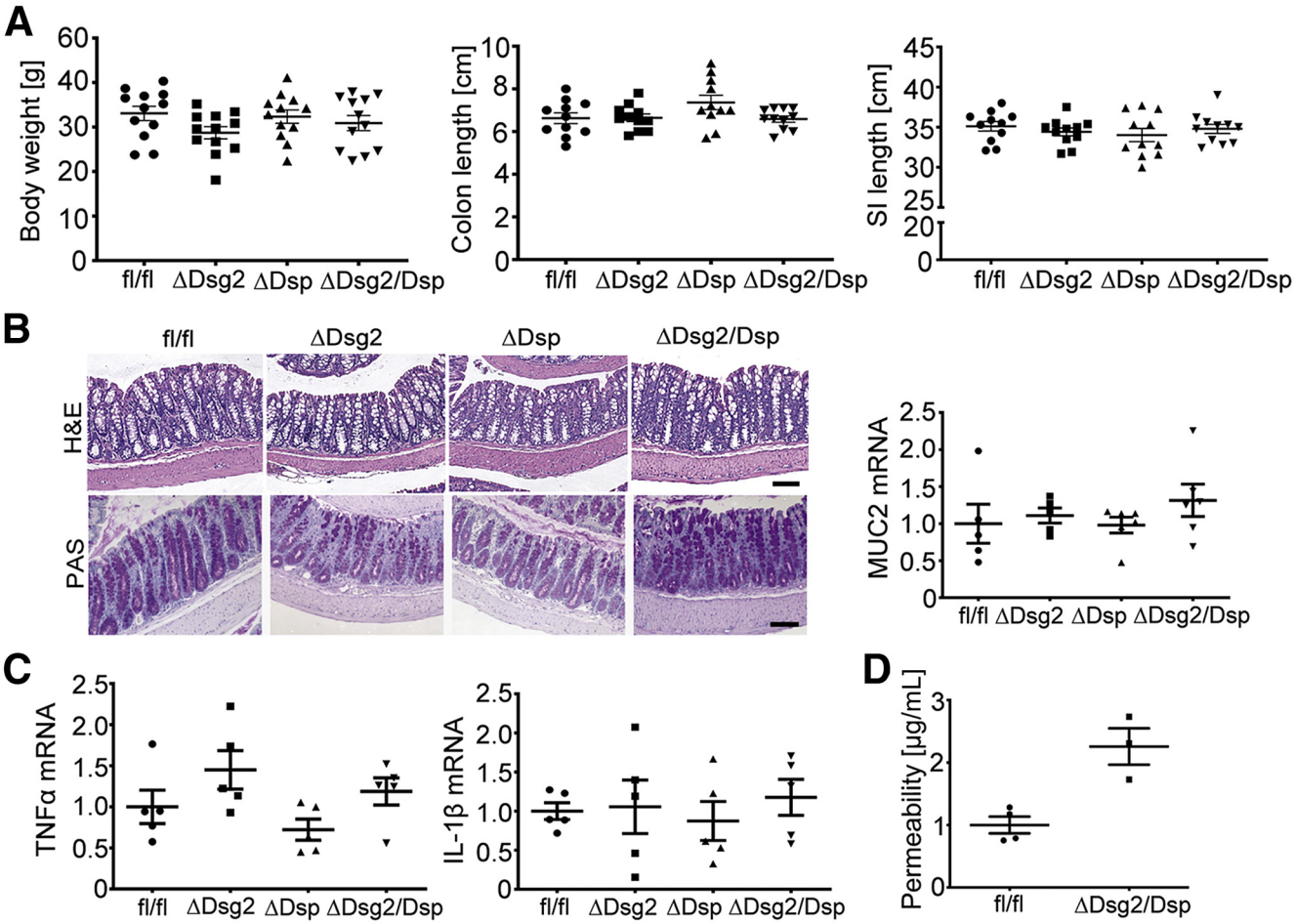

Figure 10. DSG2/DSP-deficient animals (ΔDsg2/Dsp) showed no obvious basal phenotype, but showed an increase in intestinal permeability. (*A*) The body weights and colon/small intestinal (SI) lengths of 28-week-old, sex-matched double-knockout DSG2/DSP$^{\Delta IEC}$ (ΔDsg2/Dsp) mice, single-knockout DSG2$^{\Delta IEC}$ (ΔDsg2) and DSP$^{\Delta IEC}$ (ΔDsp) animals, as well as their floxed littermates (fl/fl) were measured (n = 11–12). (*B*) The colonic architecture was assessed after H&E staining. PAS staining shows the goblet cells. The expression of the goblet cell product mucin 2 (*MUC2*) was quantified by real-time reverse-transcription polymerase chain reaction (n = 5–6). *Scale bars*: 100 μm. (*C*) The levels of inflammatory cytokines tumor necrosis factor α (*TNF*α) and *IL-1*β in colonic tissues were evaluated in 28-week-old, sex-matched mice by real-time reverse-transcription polymerase chain reaction (n = 5). The *L7* (mouse ribosomal protein) gene was used as an internal control. Average mRNA expression in fl/fl mice was set arbitrarily as 1 and levels in other genotypes represent a ratio. (*D*) Serum levels of 4-kilodalton FITC dextran were measured in 28-week-old ΔDsg2/Dsp animals and the corresponding floxed mice 4 hours after the gavage (n = 3–4). Average FITC dextran level in fl/fl mice was set arbitrarily as 1 and levels in ΔIEC mice were presented as a ratio. All data are represented as dot plots. Similar results were obtained in male and female mice.

the development was recorded with the EVOS FL Cell Imaging System (Thermo Scientific, Waltham, MA).

Biochemical Methods

To obtain the luminal content, the colon was removed and opened longitudinally. The tissue was vigorously inverted 20 times in 1× PBS. The solution was centrifuged at 5000 rpm for 10 minutes at 4°C, and the pellet was homogenized in 3% sodium dodecyl sulfate (SDS)-containing buffer supplemented with protease and phosphatase inhibitors. The protein content of the obtained luminal lysates was determined by Coomassie brilliant blue staining. Total protein lysates were prepared by direct homogenization of murine tissues or HT29 cells in an appropriate volume of 3% SDS-containing buffer. Insoluble keratin extracts were generated via high-salt extraction. Briefly, colonic tissue was homogenized in ice-cold 1% Triton X-100 (Thermo Scientific, Waltham, MA) buffer and centrifuged to obtain the supernatants constituting the soluble fraction. The pellet was homogenized in high-salt buffer (10 mmol/L Tris, pH 7.6; 140 mmol/L NaCl, 1.5 mol/L KCl; 5 mmol/L EDTA in 0.5% Triton-X) and washed to remove nucleic acids before being dissolved in 3% SDS-containing Laemmli buffer (Strnad et al, 2016).[36] The same amounts of proteins were separated by SDS-polyacrylamide gel electrophoresis followed by transfer to polyvinylidene difluoride membranes. The membranes were incubated with specific primary and horseradish-peroxidase–coupled secondary antibodies. Finally, antigen–antibody complexes were visualized by an

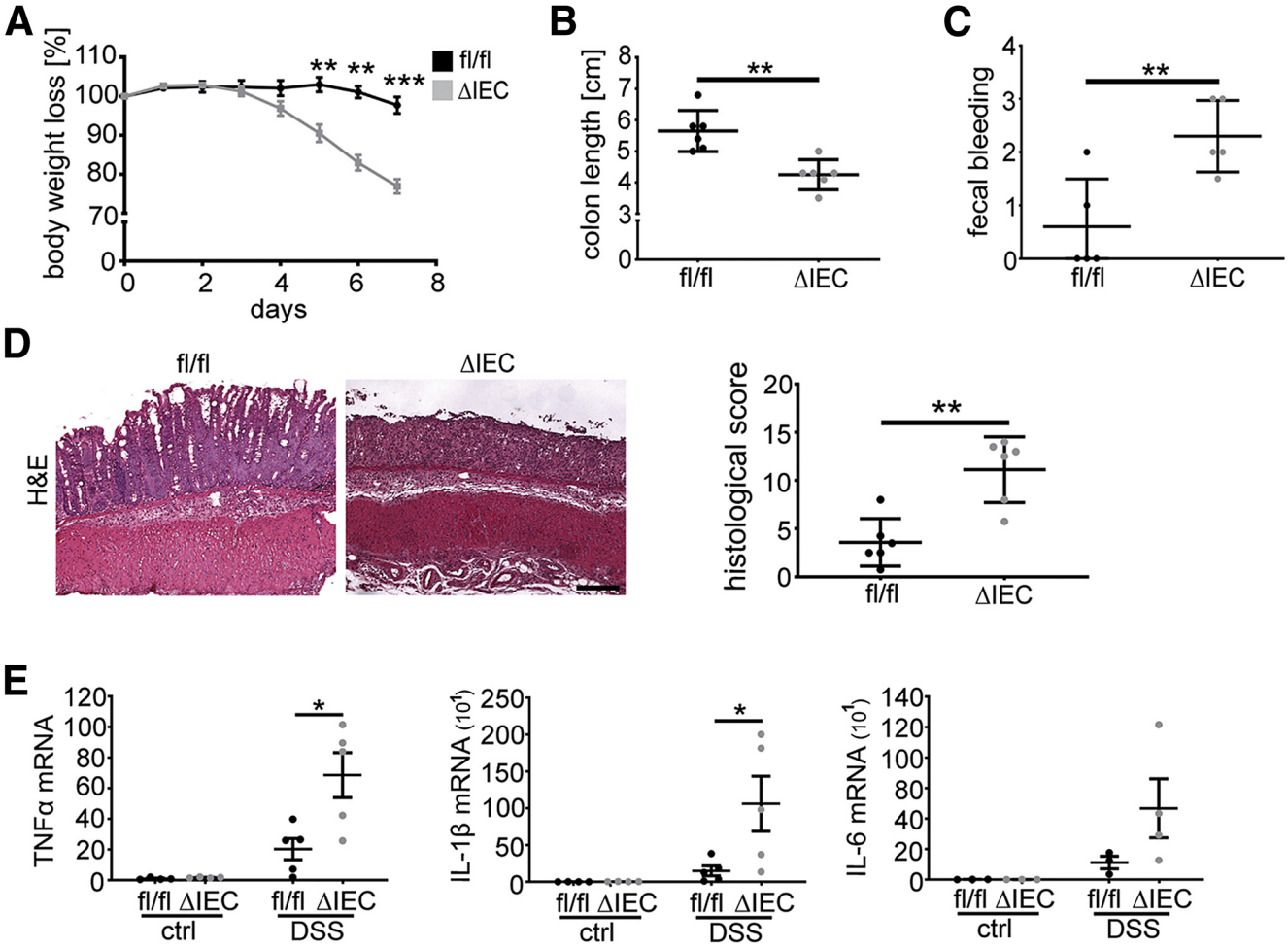

Figure 11. DSP-deficient animals (DSP$^{\Delta IEC}$) showed an enhanced susceptibility toward DSS-induced colitis. (*A*) Relative body weights of 10-week-old, sex-matched DSP$^{\Delta IEC}$ (ΔIEC) (grey rectangles) and DSP$^{fl/fl}$ (fl/fl) mice (*black circles*, n = 6 each) were evaluated daily starting at the day of first DSS administration (day 0). (*B–D*) Seven days after the first DSS administration, the severity of colitis was assessed by measuring colonic length (n = 6), semiquantitative scoring of stool blood content with guaiac test (n = 5), and H&E staining of colon sections with histologic scoring (n = 6). *Scale bar*: 100 μm. (*E*) To assess colonic inflammation, cytokines tumor necrosis factor α (*TNF*α), *IL-1*β, and *IL-6* were quantified by real-time reverse-transcription polymerase chain reaction (n = 4–5). The cytokine expression in nontreated animals (ctrl) was set arbitrarily as 1. The *L7* (mouse ribosomal protein) gene was used as an internal control. A 2-tailed Student *t* test was used for statistical analyses. **P* < .05, ***P* < .01, ****P* < .001. The data are represented as dot plots. Similar results were obtained in male and female mice.

enhanced chemiluminescence detection kit (GE Healthcare/Amersham Biosciences, Chicago, IL). The relative protein amounts were quantified by densitometry via ImageJ software (National Institutes of Health, Bethesda, MD) and depicted as optical density values. The antibodies used are summarized in Table 1.

Histologic Analysis

Formaldehyde-fixed tissues were embedded in paraffin, cut into 3-μm–thick sections, and deparaffinized for H&E and PAS staining. For the latter, slides were oxidized in 2% periodic acid solution for 5 minutes. After washing in distilled water, Schiff reagent was applied for 15 minutes, followed by hematoxylin counterstaining. Subsequently, the sections were blued in 1 mol/L Tris buffer (pH 8.0). All images were acquired and examined with a Zeiss light microscope and AxioVision Rel 4.8 software (Zeiss, Jena, Germany). PAS-positive cells were counted and presented as a mean from at least 20 assessed crypts per mouse by ImageJ software. H&E-stained, DSS-treated sections were evaluated by a previously described scoring system with minor modifications:[13] (1) submucosa thickening/edema, (2) inflammatory cell infiltration, (3) goblet cell loss (each parameter with a score of 0 to 3, as follows: 0, normal; 1, mild; 2, moderate; and 3, severe), (4) epithelial damage/erosion (0, normal; 2, <1/3 of total area with altered epithelial cell morphology; 4, >1/3 of total area with altered epithelial cell morphology and/or mild erosions; 6, <10% of ulcerative areas; 8, 10%–20% of ulcerative areas, 10, >20% of ulcerative areas). Analysis was performed in a blinded manner by P.B. (certified pathologist) and A.G.

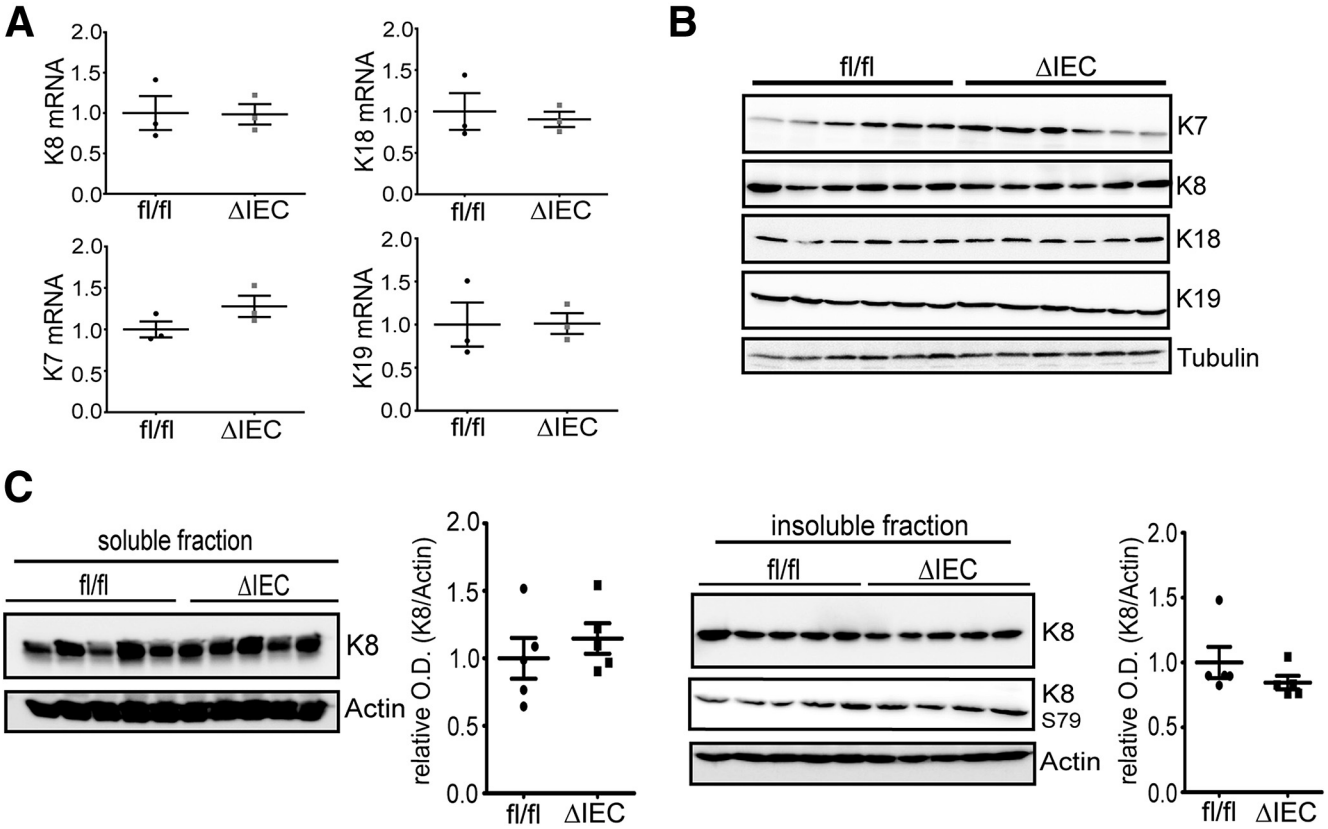

Figure 12. Loss of DSP does not affect the expression and solubility of keratins. (*A* and *B*) The mRNA and protein levels of K7, K8, K18, and K19 were assessed in the colons of 10-week-old, sex-matched $DSP^{\Delta IEC}$ (ΔIEC) mice and their floxed littermates (fl/fl) by real-time reverse-transcription polymerase chain reaction (n = 3) and immunoblotting (n = 6). (*C*) K8 solubility in 1% Triton X–containing buffer was evaluated in the colon of both groups by immunoblotting and subsequent densitometric quantification. The K8 optical density (OD) values were normalized to the OD values of β-actin (n = 5). Average levels in fl/fl mice were set arbitrarily as 1 and the amounts in ΔIEC mice were presented as a ratio. The *L7* (mouse ribosomal protein) gene is an internal control and (*B*) β-tubulin and (*C*) β-actin were used as loading controls. The data are shown as dot plots. A 2-tailed Student *t* test was used for statistical analyses. Similar results were obtained in male and female mice.

Immunohistochemistry

Immunohistochemistry staining and visualization of BrdU and Agr2 was performed on paraffin specimens, which were cut into 5-μm–thick sections. Deparaffinized slides were boiled in citrate-based antigen unmasking solution at pH 6 (Vector Laboratories, Burlingame, CA). Before blocking in 5% normal goat serum in PBS for 30 minutes, sections were incubated with 3% H_2O_2 for 10 minutes to reduce the endogenous peroxidase activity. For BrdU staining, an additional treatment with 2 N HCl for 30 minutes was performed to denature DNA, followed by neutralization with 0.1 mol/L sodium borate (pH 8) for 9 minutes. Afterward, samples were incubated with anti-BrdU or anti-Agr2 antibody overnight at 4°C. After washing, a species-specific biotinylated secondary antibody (Vector Laboratories) was applied for 1 hour, after incubation with Vectastain working solutions (Vectastain ABC Kit; Vector Laboratories). 3,3′-diaminobenzidine (Vector Laboratories) was used to develop staining and hematoxylin was applied as a counterstain. BrdU-positive cells were counted as a mean from at least 20 different crypts per mouse.

Immunofluorescence Staining

Immunofluorescence staining was performed on frozen, OCT-embedded tissues cut into 5 -μm–thick sections or HT29 cells grown on glass slides (354114, 4 wells; Falcon, Kaiserslautern, Germany). Tissue specimen and cells were fixed in precooled acetone or precooled methanol for 10 minutes, respectively. Blocking was performed for 1 hour in 2% normal goat serum, 1% bovine serum albumin (BSA), 0.1% cold fish skin gelatin, 0.1% Triton X-100, 0.05% Tween 20 in 1× PBS (tissue) or 2% BSA in phosphate-buffered saline with Tween (cells). Subsequently, samples were incubated with the following antibodies overnight at 4°C: anti-Dsg2, anti-Dsc2 (AG Leube, RWTH Aachen, Aachen, Germany),[13] anti-Dsp (CBL173; Millipore, Darmstadt, Germany) and anti–γ-catenin (Plakoglobin) (sc30997 K-20; Santa Cruz, Heidelberg, Germany). After washing, specimens were subjected to anti-goat Alexa-Fluor 488/568–conjugated secondary antibodies (Invitrogen, Molecular Probes, Eugene, OR) for 1 hour at room temperature and mounted with ProLong Gold antifade reagent containing 4′,6-diamidino-2-phenylindole (P36935; Thermo Scientific

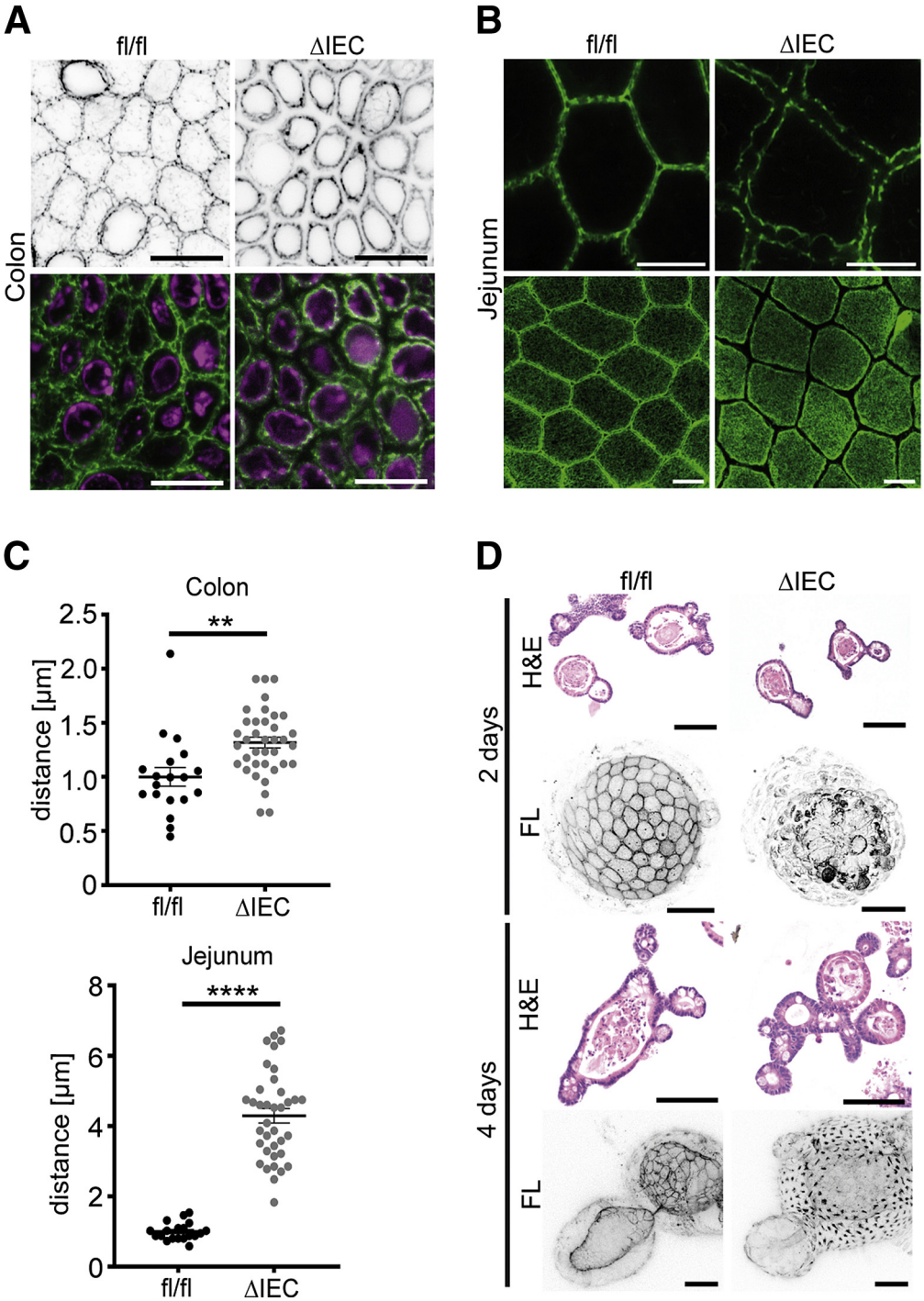

Figure 13. DSP-deficient animals showed an altered keratin network organization. (*A–C*) K8 structure was evaluated in the colon and jejunum of 10-week-old, sex-matched Dsp-deficient mice (ΔIEC) and their floxed littermates (fl/fl) producing YFP-tagged K8, with subsequent quantification of the distance between the keratin rings from individual epithelial cells (n = 19–37). Hoechst was used as a nuclear counterstain. *Scale bars*: 10 μm (colon); 5 μm (jejunum). The quantification is represented as dot plots. (*D*) Organoids were grown from small intestinal stem cells of both genotypes and assessed at days 2 and 4 of culture by H&E staining. The organization of the keratin network was visualized by fluorescence microscopy (FL). *Scale bars*: 100 μm (H&E); 20 μm (fluorescent image). A 2-tailed Student *t* test was used for statistical analyses. $^{**}P < .01$, $^{****}P < .0001$. Similar results were obtained in male and female mice.

GmbH, Schwerte, Germany). Images were acquired with a Zeiss microscope Axio Imager Z1 (Zeiss).

Quantitative Real-Time Polymerase Chain Reaction

Total RNA was isolated from tissues and HT29 cells using the RNeasy Mini Kit (Qiagen, Hilden, Germany) according to the manufacturer's instructions. A total of 1 μg RNA was reverse-transcribed into complementary DNA with the M-MLV Reverse Transcriptase Kit (Promega, Mannheim, Germany) and quantitative real-time reverse-transcription polymerase chain reaction was performed using the 7300 Fast Real-Time Polymerase Chain Reaction System (Applied Biosystems, Waltham, MA). All samples were measured in duplicate and quantified with the ΔΔCt method in relation

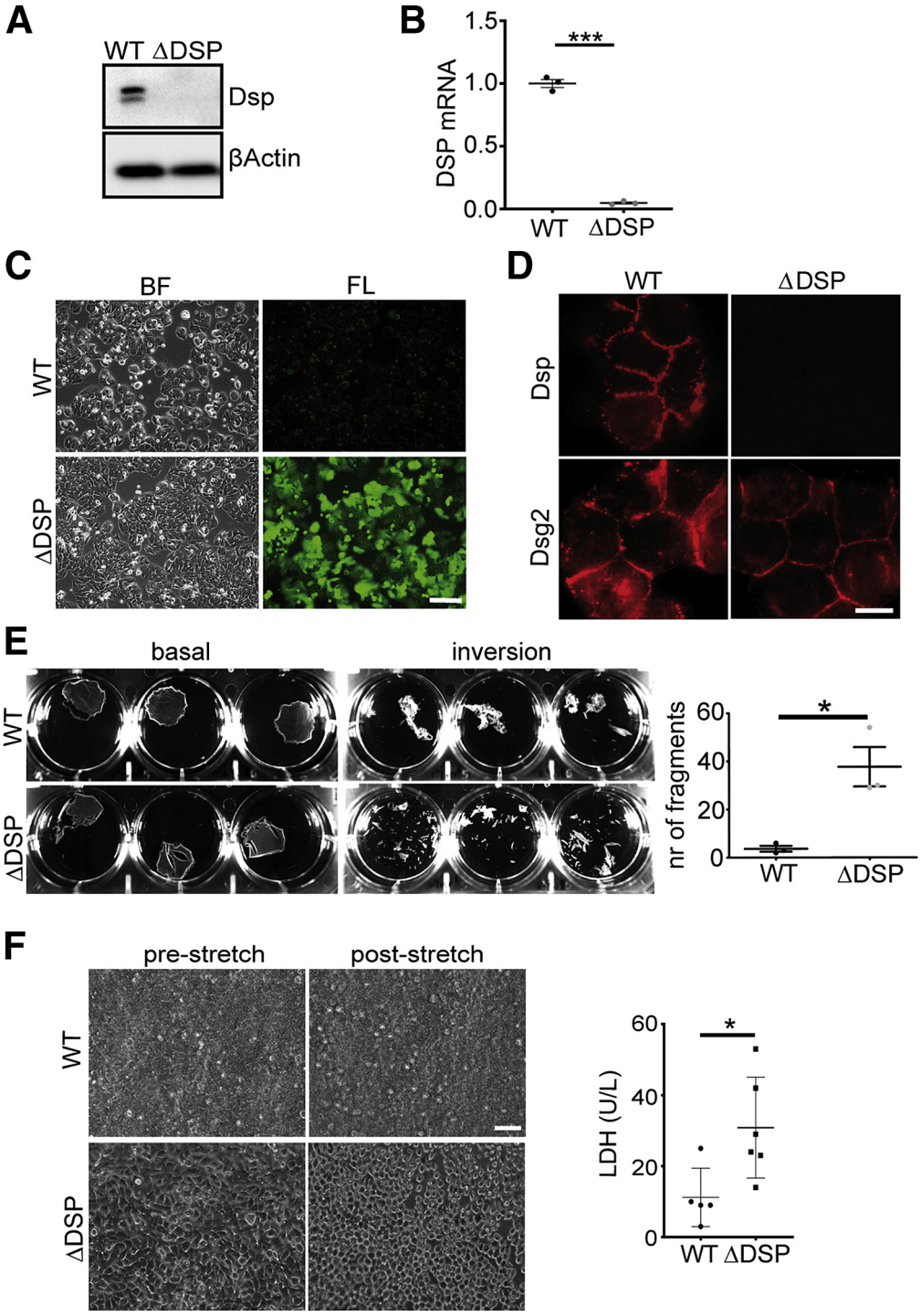

Figure 14. DSP loss results in epithelial fragility. (*A* and *B*) Dsp mRNA and protein levels were assessed in Dsp-deficient (ΔDSP) and WT HT29 cells by real-time reverse-transcription polymerase chain reaction and immunoblotting (n = 3). The *hRPLPO* gene and β-actin were used as an internal and loading control, respectively. (*C*) Autofluorescence of green fluorescent protein incorporated in the Dsp targeting construct was used to visualize the transduction efficiency. *Scale bar*: 100 μm. (*D*) The distribution of Dsp and Dsg2 was analyzed by immunofluorescence. *Scale bar*: 20 μm. (*E* and *F*) Epithelial adhesion was assessed by a dispase test with subsequent quantification of the number of epithelial sheet fragments (n = 3) and by 10 hours of cyclic stretching of cell monolayers in silicone chambers. Cells were visualized before stretch and after stretch by bright-field microscopy. *Scale bar*: 200 μm. L-Lactate dehydrogenase (LDH) was measured to determine the extent of cellular damage (n = 5–6). A 2-tailed Student *t* test was used for statistical analyses. $^{*}P < .05$, $^{***}P < .001$. BF, bright-field; FL, fluorescence; nr, number.

to the internal control (ribosomal protein L7). The primers used in the experiments are summarized in Table 2. All expression levels are represented as means ± SEM.

Transmission Electron Microscopy

Colonic tissue was cut into ~1 mm^3 pieces and fixed at room temperature with the following 3 fixatives: (1) 3.7% formaldehyde, 1% glutaraldehyde, 11.6 g $NaH_2PO_4xH_2O$ and 2.7 g NaOH per liter ddH_2O for 2 hours; (2) 1% OsO4 for 1 hour; and (3) 0.5% uranylacetate/0.05 N sodium hydrogen maleate (pH 5.2) for 2 hours. Subsequently, samples were dehydrated, embedded in araldite for 48 hours at 60°C, and cut into 75-nm ultrathin sections. To enhance the contrast, sections were treated with 3% uranylacetate for 4 minutes and with 80 mmol/L lead citrate for 3 minutes. Images were

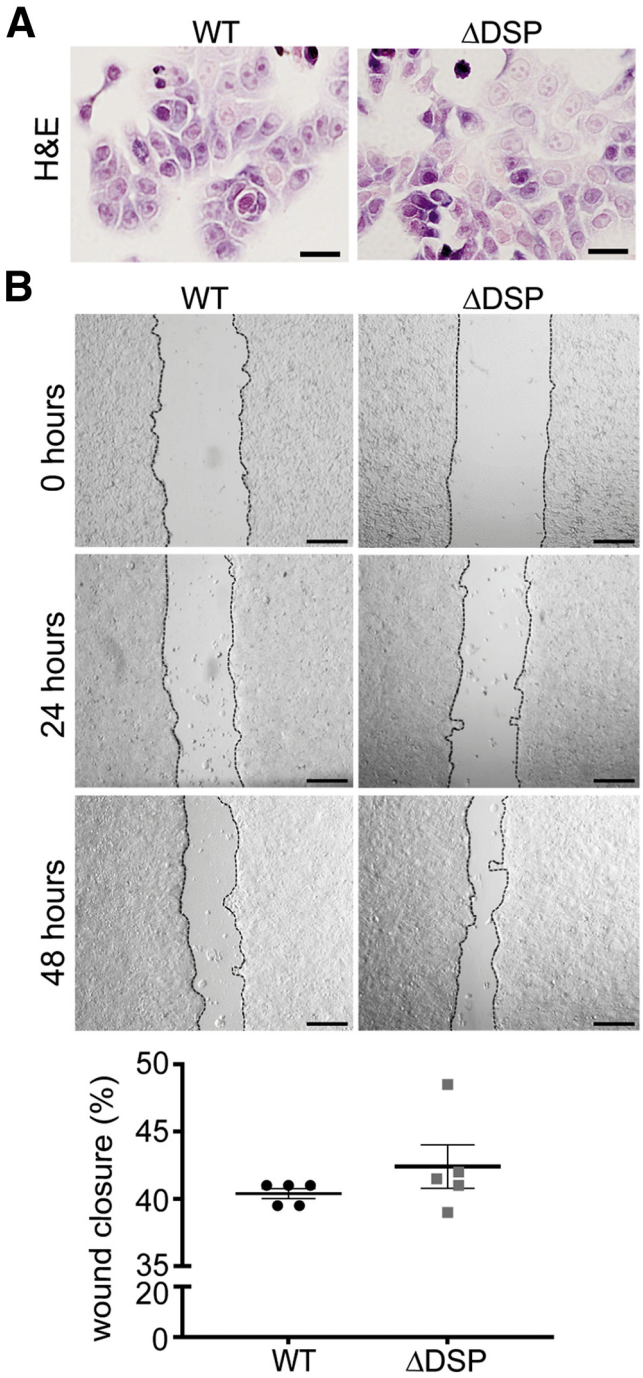

Figure 15. DSP-deficient animals (DSP$^{\Delta IEC}$) showed no alterations in wound healing. (*A*) Monolayer formation was confirmed via H&E staining in Dsp-deficient (ΔDSP) and WT HT29 cells. *Scale bars*: 20 μm. (*B*) Cell migration was assessed by wound healing assay with subsequent quantification of the wound closure area (%) after 48 hours in both groups (n = 5). Cells were visualized 24 and 48 hours after wound scratching by bright-field microscopy. *Scale bars*: 200 μm. The data are represented as dot plots. A 2-tailed Student *t* test was used for statistical analyses.

acquired with an EM 10 (Zeiss) plus digital camera (Olympus, Hamburg, Germany) and the corresponding iTEM software (Olympus).

Ex Vivo Microscopy

Colons and jejuna from DSP$^{\Delta IEC}$/K8–YFP knock-in mice were flushed with PBS, opened longitudinally, and transferred to glass-bottom dishes (MatTek, Ashland, MA) containing prewarmed Krebs–Henseleit buffer (114 mmol/L NaCl, 5 mmol/L KCl, 24 mmol/L $NaHCO_3$, 1 mmol/L $MgCl_2$, 2.2 mmol/L $CaCl_2$, 10 mmol/L HEPES, 0.25% BSA, pH 7.35). A total of 2.5 μg/mL Hoechst33342 was added for staining of the nuclei in colonic tissue. Organoids were grown on glass-bottom dishes and overlayed with the Hoechst33342-containing Krebs–Henseleit buffer. Images were acquired with a Zeiss LSM710 Duo microscope, a 405-nm diode laser, an argon ion laser at 488 nm, and a 63×/1.4 Numerical aperture DIC M27 oil immersion objective at 37°C. In addition, the Airyscan detector in super-resolution mode was used. Images were deconvoluted using Zen black software (Zeiss, Wetzlar, Germany) and processed using Fiji.[38] The distance between the keratin rings of individual cells was quantified via Fiji.

Cell Culture Experiments

A human colon adenocarcinoma cell line (HT29, ATCC HTB-38; LGC Standards GmbH, Wesel, Germany) with a stable DSP knockdown was generated using the CRISPR/Cas system.[39] Briefly, short guide RNA, which targets exon 8 of the DSP gene (for additional information see Table 2), was designed using the Broad Institute (Cambridge, MA) platform and integrated into the vector pL-CRISPR.EFS.GFP (Addgene, Watertown, MA) for lentiviral delivery. The construct was amplified in competent Stbl3 *Escherichia coli* (Invitrogen) and the GeneJET plasmid miniprep and maxiprep kits were used for its isolation (Thermo Scientific). For the production of lentiviral particles, HEK293T cells were co-transfected with lentiviral envelope plasmid (pMD2.G; Addgene Europe, Teddington, UK), packaging plasmid (psPAX2; Addgene Europe), and the previously generated vector using TransIT-LT1 transfection reagent (Mirusbio, Goettingen, Germany). After 48 hours, the lentiviral particles were collected by centrifugation of the cell culture supernatant at 1500 rpm for 5 minutes and filtration with a 45-μm pore size filter. Finally, target HT29 cells were transduced with the isolated particles. Fluorescence-activated cell sorting was used to select transfected, GFP-expressing cells. HT29 cells were cultured in a complete culture medium (RPMI 1640; PAN Biotech, Bavaria, Germany) containing 10% fetal bovine serum and 1% (50 U/mL) penicillin-streptomycin (PAN biotech) in a 5% CO_2 atmosphere at 37°C until they reached confluence. For H&E staining, WT and GFP-expressing Dsp-deficient HT29 cells were seeded on chamber slides (Thermo Scientific) and fixed in 4% paraformaldehyde. Images were acquired with an Axio Vert.A1 (Zeiss).

Dispase Assay

Dsp-deficient and WT HT29 cells were seeded into 6-well plates. After reaching confluency, cells were washed in PBS and Hank`s balanced salt solution (P04-

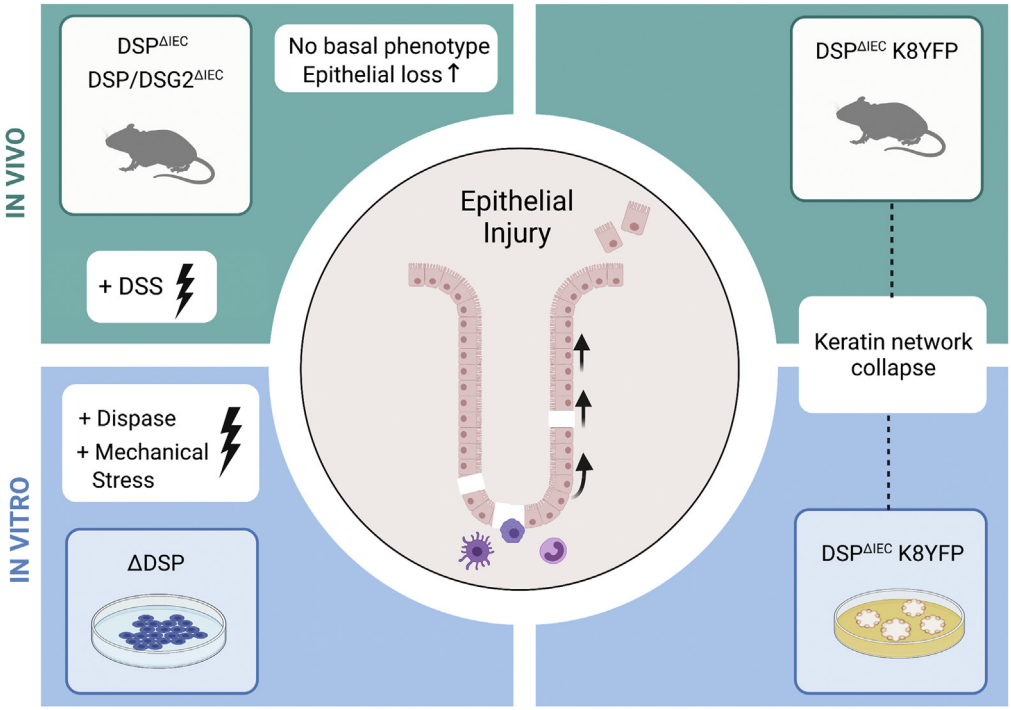

Figure 16. Schematic summarizing the findings of the study. Dsp- and Dsg2/Dsp-deficient mice showed no basal phenotype, but an increased permeability, epithelial loss into the intestinal lumen, and faster migration. In DSP$^{\Delta IEC}$ mice, treatment with DSS lead to increased intestinal injury with strong inflammatory response. Cross-breeding with K8–YFP knock-in mice and assessment of the tissues as well as small intestinal organoids showed a collapsed keratin network with loss of desmosomal anchorage. Dsp knock-down in vitro resulted in susceptibility to mechanical injury and impaired cell adhesion.

34500; PAN Biotech). Afterward, incubation with 3.6 U/mL dispase II in Hank`s balanced salt solution (Roche, Mannheim, Germany) at 37°C for 30 minutes was performed to release cellular monolayers from the plate bottom. The epithelial sheets were subjected to mechanical stress by inversion on a tube rotator (444-0500; VWR, Radnor, PA) for 5 minutes at 18 rpm and the resulting fragments were counted by an ImageQuant AS 4000 camera system equipped with ImageQuant software (GE Healthcare Europe GmbH, Freiburg, Germany).

Cell Stretching

To perform cyclic stretch experiments, 0.3×10^6 Dsp-deficient or WT HT29 cells were seeded on elastic polydimethylsiloxane chambers (silicone elastomers, SYLGARD, 184; Dow Chemical Company, Midland, MI) that were coated with 100 μg/mL fibronectin. After reaching more than 80% confluence, chambers were placed into an automatic cell chamber stretcher and a simultaneous, linear, uniaxial stretch with 35% stretching strength and a frequency of 0.3 Hz was conducted for 10 hours.[40] To analyze the impact of stretching on cellular adhesion,

Table 1. Antibodies Used for Western Blot

Antibody	Host	Company
Anterior gradient 2 (EPR20164-278)	Rabbit	ab209224; Abcam, Cambridge, UK
Desmocollin 2	Guinea pig	Institute of Molecular and Cellular Anatomy, RWTH Aachen, Germany
Desmoglein 2	Rabbit	Institute of Molecular and Cellular Anatomy, RWTH Aachen, Germany
Desmoplakin I/II	Rabbit	sc33555 (H-300); Santa Cruz
Desmoplakin I/II (clone DP 2.15)	Mouse	CBL173; Millipore
Keratin 7 (RCK105)	Mouse	ab9021; Abcam
Keratin 8 (clone Ks.8.7)	Mouse	61038; Progen, Heidelberg, Germany
Keratin 8 (S79)	Mouse	LJ4[37]
Keratin 18 (clone Ks 18.04)	Mouse	61028; Progen
Keratin 19 (TROMAIII)	Rat	Developmental Studies Hybridoma Bank; Iowa City, IA
Plakophilin 2	Goat	ab189323
β-actin	Mouse	A2228; Sigma-Aldrich
β-tubulin	Mouse	T8328; Sigma-Aldrich
γ-catenin (PG)	Goat	sc30997 (K-20); Santa Cruz

monolayers were examined by bright-field microscopy before and after stretching. To quantify the extent of cellular damage, lactate dehydrogenase levels were measured in the supernatant.

Wound Healing Assay

Dsp-deficient and WT HT29 cells were seeded into 12-well plates. After reaching confluency, a pipette tip was used to scratch a wound (straight line) into the cell

Table 2. Primers Used for Genotyping, Quantitative Real-Time Polymerase Chain Reaction, and CRISPR/Cas

Genotyping polymerase chain reaction primer		
mDsg2	Forward	GGTAAATGCAGACGGATCAG
	Reverse	TGGGCTACACTCATAGGAAG
mDsp	Forward	TGTCTGTTGCCATGTGATGCC
	Reverse	GACTTGGACGATCGCCTTCTG
mVillin-Cre	Forward	CCACGACCAAGTGACAGCAAT
	Reverse	TTCGGATCATCAGCTACACCA
mK8YFP	Forward	ACGTAAACGGCCACA
	Reverse	AAGTCGTGCTGCTTC
Quantitative real-time polymerase chain reaction primer		
mutE4/E5-mDsg2	Forward	ACCGGGAAGAAACACCATATT
	Reverse	AGGGCTTTTCCAGGTTGTTT
mDsc2	Forward	GCACTGGTCGTGTAGATCGT
	Reverse	CTCTGGCGTATACCCATCTG
mPG/JUP	Forward	TCCTGCACAACCTCTCTCAC
	Reverse	ACTGAGCATTCGGACTAGGG
mDSP	Forward	CTGGCAAACGAGACAAATCA
	Reverse	GATGCCAGCTGCAGTTCATA
mPkp2	Forward	TCAGCATACACGGAAGATGC
	Reverse	GGGAAAGATTCCGTGACAAA
mK7	Forward	ACGGCTGCTGAGAATGAGTT
	Reverse	CGTGAAGGGTCTTGAGGAAG
mK8	Forward	GGACATCGAGATCACCACCT
	Reverse	TGAAGCCAGGGCTAGTGAGT
mK18	Forward	CAAGTCTGCCGAAATCAGGGAC
	Reverse	TCCAAGTTGATGTTCTGGTTTT
mK19	Forward	ACCTACCTTGCTCGGATTGA
		CGTGACTTCGGTCTTGCTTA
	Reverse	CGTGACTTCGGTCTTGCTTA
mMuc2	Forward	GCTGACGAGTGGTTCGTGAATG
	Reverse	GATGAGGTGGCAGACAGGAGAC
mSpdef	Forward	CTTCATCCGCTGGCTCAACA
	Reverse	CGGGTTTACGAATGATGCCC
mGfi1	Forward	GACTCTCAGCTTACCGAGGC
	Reverse	TGCATAGGGCTTGAAAGGCA
mAtoh1	Forward	AGCTTCCTCTGGGGGTTACT
	Reverse	TTCTGTGCCATCATCGCTGT
mHes1	Forward	CTGGTGCTGATAACAGCGGA
	Reverse	AGGGCTACTTAGTGATCGGT
mTNFa	Forward	TCAGCCTCTTCTCATTCCTGCTT
	Reverse	AGGCCATTTGGGAACTTCTCATC
mIL1b	Forward	TGAAGCAGCTATGGCAACTG
	Reverse	GGGTCCGTCAACTTCAAAGA
mIL6	Forward	ACAAAGCCAGAGTCCTTCAGAGAGA
	Reverse	TGGTCTTGGTCCTTAGCCACTCC
mL7	Forward	GAAAGGCAAGGAGGAAGCTCATCT
	Reverse	AATCTCAGTGCGGTACATCTGCCT
CRISPR/Cas primer		
hDSP (exon 8)	CAACG+ forward	CTGGCAAACGAGACAAATCA
NM_001008844	AAAC + reverse	GATGCCAGCTGCAGTTCATA

h, human; m, mouse.

monolayer followed by a washing step in 1× PBS to remove detached cells. To analyze cell migration, wound closure was tracked by bright-field microscope before and 24/48 hours after scratching. Surface area measurements (wound closure %) were conducted via ImageJ software.

Study Approval

The animal experiments were approved by the state of North Rhine-Westphalia in Germany and the University of Aachen Animal Care Committee and were conducted in compliance with the German Law for Welfare of Laboratory Animals.

Data Analysis and Statistical Methods

Image quantifications were performed with ImageJ. Data were analyzed with an unpaired 2-tailed Student *t* test or 1-way analysis of variance. Two-tailed *P* values less than .05 were considered statistically significant. All authors had access to the study data and reviewed and approved the final manuscript.

References

1. Etienne-Manneville S. Cytoplasmic intermediate filaments in cell biology. Annu Rev Cell Dev Biol 2018; 34:1–28.
2. Jacob JT, Coulombe PA, Kwan R, Omary MB. Types I and II keratin intermediate filaments. Cold Spring Harb Perspect Biol 2018;10:a018275.
3. Hatzfeld M, Keil R, Magin TM. Desmosomes and intermediate filaments: their consequences for tissue mechanics. Cold Spring Harb Perspect Biol 2017; 9:a029157.
4. Rubsam M, Broussard JA, Wickstrom SA, Nekrasova O, Green KJ, Niessen CM. Adherens junctions and desmosomes coordinate mechanics and signaling to orchestrate tissue morphogenesis and function: an evolutionary perspective. Cold Spring Harb Perspect Biol 2018;10:a029207.
5. Broussard JA, Jaiganesh A, Zarkoob H, Conway DE, Dunn AR, Espinosa HD, Janmey PA, Green KJ. Scaling up single-cell mechanics to multicellular tissues - the role of the intermediate filament-desmosome network. J Cell Sci 2020;133:jcs228031.
6. Holthofer B, Windoffer R, Troyanovsky S, Leube RE. Structure and function of desmosomes. Int Rev Cytol 2007;264:65–163.
7. Coulombe PA. The molecular revolution in cutaneous biology: keratin genes and their associated disease: diversity, opportunities, and challenges. J Invest Dermatol 2017;137:e67–e71.
8. Norgett EE, Hatsell SJ, Carvajal-Huerta L, Cabezas JC, Common J, Purkis PE, Whittock N, Leigh IM, Stevens HP, Kelsell DP. Recessive mutation in desmoplakin disrupts desmoplakin-intermediate filament interactions and causes dilated cardiomyopathy, woolly hair and keratoderma. Hum Mol Genet 2000; 9:2761–2766.
9. Spindler V, Eming R, Schmidt E, Amagai M, Grando S, Jonkman MF, Kowalczyk AP, Muller EJ, Payne AS, Pincelli C, Sinha AA, Sprecher E, Zillikens D, Hertl M, Waschke J. Mechanisms causing loss of keratinocyte cohesion in pemphigus. J Invest Dermatol 2018; 138:32–37.
10. Ku NO, Strnad P, Bantel H, Omary MB. Keratins: biomarkers and modulators of apoptotic and necrotic cell death in the liver. Hepatology 2016;64:966–976.
11. Mathai SK, Pedersen BS, Smith K, Russell P, Schwarz MI, Brown KK, Steele MP, Loyd JE, Crapo JD, Silverman EK, Nickerson D, Fingerlin TE, Yang IV, Schwartz DA. Desmoplakin variants are associated with idiopathic pulmonary fibrosis. Am J Respir Crit Care Med 2016;193:1151–1160.
12. Polari L, Alam CM, Nystrom JH, Heikkila T, Tayyab M, Baghestani S, Toivola DM. Keratin intermediate filaments in the colon: guardians of epithelial homeostasis. Int J Biochem Cell Biol 2020;129:105878.
13. Gross A, Pack LAP, Schacht GM, Kant S, Ungewiss H, Meir M, Schlegel N, Preisinger C, Boor P, Guldiken N, Krusche CA, Sellge G, Trautwein C, Waschke J, Heuser A, Leube RE, Strnad P. Desmoglein 2, but not desmocollin 2, protects intestinal epithelia from injury. Mucosal Immunol 2018;11:1630–1639.
14. Schlegel N, Boerner K, Waschke J. Targeting desmosomal adhesion and signalling for intestinal barrier stabilization in inflammatory bowel diseases-lessons from experimental models and patients. Acta Physiol (Oxf) 2021;231:e13492.
15. Raya-Sandino A, Luissint AC, Kusters DHM, Narayanan V, Flemming S, Garcia-Hernandez V, Godsel LM, Green KJ, Hagen SJ, Conway DE, Parkos CA, Nusrat A. Regulation of intestinal epithelial intercellular adhesion and barrier function by desmosomal cadherin desmocollin-2. Mol Biol Cell 2021; 32:753–768.
16. Habtezion A, Toivola DM, Butcher EC, Omary MB. Keratin-8-deficient mice develop chronic spontaneous Th2 colitis amenable to antibiotic treatment. J Cell Sci 2005; 118:1971–1980.
17. Vasioukhin V, Bowers E, Bauer C, Degenstein L, Fuchs E. Desmoplakin is essential in epidermal sheet formation. Nat Cell Biol 2001;3:1076–1085.
18. Krausova A, Buresova P, Sarnova L, Oyman-Eyrilmez G, Skarda J, Wohl P, Bajer L, Sticova E, Bartonova L, Pacha J, Koubkova G, Prochazka J, Sporrer M, Durrbeck C, Stehlikova Z, Vit M, Ziolkowska N, Sedlacek R, Jirak D, Kverka M, Wiche G, Fabry B, Korinek V, Gregor M. Plectin ensures intestinal epithelial integrity and protects colon against colitis. Mucosal Immunol 2021;14:691–702.
19. Schwarz N, Windoffer R, Magin TM, Leube RE. Dissection of keratin network formation, turnover and reorganization in living murine embryos. Sci Rep 2015; 5:9007.
20. Sumigray KD, Lechler T. Desmoplakin controls microvilli length but not cell adhesion or keratin organization in the intestinal epithelium. Mol Biol Cell 2012;23:792–799.

21. Price AJ, Cost AL, Ungewiss H, Waschke J, Dunn AR, Grashoff C. Mechanical loading of desmosomes depends on the magnitude and orientation of external stress. Nat Commun 2018;9:5284.
22. Garcia-Gras E, Lombardi R, Giocondo MJ, Willerson JT, Schneider MD, Khoury DS, Marian AJ. Suppression of canonical Wnt/beta-catenin signaling by nuclear plakoglobin recapitulates phenotype of arrhythmogenic right ventricular cardiomyopathy. J Clin Invest 2006; 116:2012–2021.
23. Coulombe PA, Kerns ML, Fuchs E. Epidermolysis bullosa simplex: a paradigm for disorders of tissue fragility. J Clin Invest 2009;119:1784–1793.
24. Flemming S, Luissint AC, Kusters DHM, Raya-Sandino A, Fan S, Zhou DW, Hasegawa M, Garcia-Hernandez V, Garcia AJ, Parkos CA, Nusrat A. Desmocollin-2 promotes intestinal mucosal repair by controlling integrin-dependent cell adhesion and migration. Mol Biol Cell 2020;31:407–418.
25. Wanuske MT, Brantschen D, Schinner C, Studle C, Walter E, Hiermaier M, Vielmuth F, Waschke J, Spindler V. Clustering of desmosomal cadherins by desmoplakin is essential for cell-cell adhesion. Acta Physiol (Oxf) 2021;231:e13609.
26. Cabral RM, Tattersall D, Patel V, McPhail GD, Hatzimasoura E, Abrams DJ, South AP, Kelsell DP. The DSPII splice variant is crucial for desmosome-mediated adhesion in HaCaT keratinocytes. J Cell Sci 2012; 125:2853–2861.
27. Norgett EE, Lucke TW, Bowers B, Munro CS, Leigh IM, Kelsell DP. Early death from cardiomyopathy in a family with autosomal dominant striate palmoplantar keratoderma and woolly hair associated with a novel insertion mutation in desmoplakin. J Invest Dermatol 2006; 126:1651–1654.
28. Broussard JA, Yang R, Huang C, Nathamgari SSP, Beese AM, Godsel LM, Hegazy MH, Lee S, Zhou F, Sniadecki NJ, Green KJ, Espinosa HD. The desmoplakin-intermediate filament linkage regulates cell mechanics. Mol Biol Cell 2017;28:3156–3164.
29. Snider NT, Omary MB. Post-translational modifications of intermediate filament proteins: mechanisms and functions. Nat Rev Mol Cell Biol 2014;15:163–177.
30. Geisler F, Leube RE. Epithelial intermediate filaments: guardians against microbial infection? Cells 2016;5:29.
31. Spazierer D, Fuchs P, Reipert S, Fischer I, Schmuth M, Lassmann H, Wiche G. Epiplakin is dispensable for skin barrier function and for integrity of keratin network cytoarchitecture in simple and stratified epithelia. Mol Cell Biol 2006;26:559–568.
32. Kojouharoff G, Hans W, Obermeier F, Mannel DN, Andus T, Scholmerich J, Gross V, Falk W. Neutralization of tumour necrosis factor (TNF) but not of IL-1 reduces inflammation in chronic dextran sulphate sodium-induced colitis in mice. Clin Exp Immunol 1997; 107:353–358.
33. Turner JR. Intestinal mucosal barrier function in health and disease. Nat Rev Immunol 2009;9:799–809.
34. Capaldo CT, Nusrat A. Cytokine regulation of tight junctions. Biochim Biophys Acta 2009;1788:864–871.
35. Spindler V, Meir M, Vigh B, Flemming S, Hutz K, Germer CT, Waschke J, Schlegel N. Loss of desmoglein 2 contributes to the pathogenesis of Crohn's disease. Inflamm Bowel Dis 2015;21:2349–2359.
36. Strnad P, Guldiken N, Helenius TO. Simple Epithelial Keratins. Methods Enzymol 2016;568:351–388.
37. Liao J, Ku NO, Omary MB. Stress, apoptosis, and mitosis induce phosphorylation of human keratin 8 at Ser-73 in tissues and cultured cells. J Biol Chem 1997; 272:17565–17573.
38. Schindelin J, Arganda-Carreras I, Frise E, Kaynig V, Longair M, Pietzsch T, Preibisch S, Rueden C, Saalfeld S, Schmid B, Tinevez JY, White DJ, Hartenstein V, Eliceiri K, Tomancak P, Cardona A. Fiji: an open-source platform for biological-image analysis. Nat Methods 2012;9:676–682.
39. Cong L, Ran FA, Cox D, Lin S, Barretto R, Habib N, Hsu PD, Wu X, Jiang W, Marraffini LA, Zhang F. Multiplex genome engineering using CRISPR/Cas systems. Science 2013;339:819–823.
40. Faust U, Hampe N, Rubner W, Kirchgessner N, Safran S, Hoffmann B, Merkel R. Cyclic stress at mHz frequencies aligns fibroblasts in direction of zero strain. PLoS One 2011;6:e28963.

Received August 5, 2021. Accepted December 10, 2021.

Correspondence
Address correspondence to: Pavel Strnad, MD, Department of Internal Medicine III, University Hospital Aachen, Pauwelsstraße 30, D-52074, Aachen, Germany e-mail: pstrnad@ukaachen.de.

Acknowledgments
The authors are thankful to the expert technical assistance of Ingrid Breuer, Sabine Eisner, and Christina Linnartz.

Data Availability
The original data sets generated or analyzed during the present study are available from the corresponding author on reasonable request.

CRediT Authorship Contributions

Annika Gross, Dr (Conceptualization: Equal; Data curation: Lead; Formal analysis: Lead; Funding acquisition: Supporting; Investigation: Lead; Supervision: Equal; Validation: Equal; Writing – original draft: Equal)

Biaohuan Zhou, Dr (Data curation: Supporting; Formal analysis: Supporting; Investigation: Supporting; Validation: Supporting)

Lisa Bewersdorf (Data curation: Supporting; Formal analysis: Supporting; Investigation: Supporting; Validation: Supporting)

Nicole Schwarz, Dr (Data curation: Supporting; Investigation: Supporting; Visualization: Supporting)

Gabriel M. Schacht (Data curation: Supporting; Investigation: Supporting; Validation: Supporting)

Peter Boor, Prof (Conceptualization: Supporting; Data curation: Supporting; Formal analysis: Supporting; Funding acquisition: Supporting; Resources: Supporting; Writing – review & editing: Supporting)

Konrad Hoeft, Dr (Conceptualization: Supporting; Methodology: Supporting)

Bernd Hoffmann, Dr (Methodology: Supporting; Supervision: Supporting)

Elaine Fuchs, Prof (Resources: Supporting)

Rafael Kramann, Prof (Methodology: Supporting; Resources: Supporting; Writing – review & editing: Supporting)

Rudolf Merkel, Prof (Methodology: Supporting; Resources: Supporting)

Rudolf E. Leube, Prof (Conceptualization: Supporting; Funding acquisition: Supporting; Resources: Supporting; Validation: Supporting; Visualization: Supporting; Writing – review & editing: Supporting)

Pavel Strnad, Prof (Conceptualization: Lead; Formal analysis: Supporting; Funding acquisition: Lead; Methodology: Equal; Project administration: Equal; Resources: Lead; Supervision: Equal; Writing – original draft: Equal)

Conflicts of interest
The authors disclose no conflicts.

Funding
Supported by the START program of the medical faculty at Rheinisch-Westfaelische Technische Hochschule (RWTH) Aachen University (A.G.); the Deutsche Forschungsgemeinschaft consortium Sonderforschungsbereich (SFB) 1382 "Gut-Liver Axis" (ID 403224013) and Deutsche Forschungsgemeinschaft grant STR1095/6-1 (P.S.); Deutsche Forschungsgemeinschaft (German Research Foundation, Project-IDs 322900939, 454024652, 432698239, 445703531), the European Research Council (ERC, Consolidator Grant No 101001791), and the Federal Ministry of Education and Research (STOP-FSGS-01GM1901A) (P.B.); Deutsche Forschungsgemeinschaft (LE566/22-2/SPP1782 and 363055819/GRK2415) (R.L.) and National Institutes of Health NIAMS R01-AR27883 (E.F.).